

2017

On The Microstructural Behavior of Pure Magnesium Under Various Strain Rates

Peter Malchow
University of South Carolina

Follow this and additional works at: <https://scholarcommons.sc.edu/etd>



Part of the [Mechanical Engineering Commons](#)

Recommended Citation

Malchow, P.(2017). *On The Microstructural Behavior of Pure Magnesium Under Various Strain Rates*. (Master's thesis). Retrieved from <https://scholarcommons.sc.edu/etd/4483>

This Open Access Thesis is brought to you by Scholar Commons. It has been accepted for inclusion in Theses and Dissertations by an authorized administrator of Scholar Commons. For more information, please contact digres@mailbox.sc.edu.

ON THE MICROSTRUCTURAL BEHAVIOR OF PURE MAGNESIUM UNDER
VARIOUS STRAIN RATES

by

Peter Malchow

Bachelor of Science
University of Wisconsin-River Falls, 2015

Submitted in Partial Fulfillment of the Requirements

For the Degree of Master of Science in

Mechanical Engineering

College of Engineering and Computing

University of South Carolina

2017

Accepted by:

Addis Kidane, Director of Thesis

Anthony Reynolds, Reader

Cheryl L. Addy, Vice Provost and Dean of the Graduate School

© Copyright by Peter Malchow, 2017
All Rights Reserved.

ACKNOWLEDGEMENTS

First and foremost, I would like to acknowledge my academic and research advisor Dr. Addis Kidane for his support and leadership throughout my graduate career here at the University of South Carolina. His direction and guidance has helped me develop a refined work ethic and natural curiosity for the fields of engineering and mechanics.

I would also like to acknowledge Dr. Anthony Reynolds for sharing his advice and valued insight with regards to scope of this work and for his overall expertise in field of material science engineering.

Mr. Suraj Ravindran is acknowledged here for providing invaluable experimental knowledge for numerous projects and helping lay the foundation for all of my experimental work. Mr. Ravindran displays one of the highest levels of capability and talent in the discipline of experimental works I have ever had the honor of working with.

I also acknowledge Mr. Behrad Koohbor for his intellectual input toward our experimental approach and for sharing with me the base knowledge for being a proficient scientific communicator. Mr. Koohbor has lead by example as one of the most prolific and skilled researchers I had the distinct privilege of collaborating with.

Finally, I would like to acknowledge Mr. Burton Kotti for his valued assistance in my experimental work during the latter part of my academic career at this institution.

ABSTRACT

An investigation into the localized microstructural response of pure magnesium under both quasi-static and dynamic loading is presented in the form of several experimental works. The meso-scale events were examined using Digital Image Correlation techniques, which provide a methodology for mapping the in-situ full-field material strain behavior.

Firstly, an analysis of the grain boundary activity specifically under dynamic conditions at high magnification is discussed. An area of interest in the region of multiple grain boundaries and triple junctions is selected for characterizing the evolution of the strain and local rotation. This is followed by a study experimentally verifying the causes of the material failure in the quasi-static case, while simultaneously accounting for the effects of grain arrangement on the global response and quantifying the contributions of both inter and intragranular deformation. Finally, we discuss the variations in the localized strain patterns of rolled magnesium under tension with respect to the multi-scale grain sizes in the material, and the local deformation characteristics which are possibly affected.

In summary, the influence of various granular properties was correlated with the full-field material response and the structurally weak regions of the material were identified. In all scenarios tested, it was verified that the grain boundaries were mechanically weak and fracture initiation took place primarily in these regions. Additionally, the intergranular deformation quantified in the dynamic regime was seen to occur preferentially at triple junction points.. Lastly, it was observed that large relative differences in grain size within

a single specimen may dictate the locations of mechanically susceptible failure points in the microstructure, as well as the formation of possible deformation mechanisms.

TABLE OF CONTENTS

ACKNOWLEDGEMENTS	iii
ABSTRACT	iv
LIST OF FIGURES	vii
LIST OF ABBREVIATIONS	ix
CHAPTER 1: INTRODUCTION.....	1
CHAPTER 2: OVERVIEW OF MAGNESIUM PROPERTIES.....	7
CHAPTER 3: ON THE IN-SITU LOCALIZED DEFORMATION BEHAVIOR OF PURE MAGNESIUM UNDER DYNAMIC LOADING.....	15
CHAPTER 4: IN-SITU QUANTIFICATION OF INTRA AND INTERGRANULAR DEFORMATION IN PURE MAGNESIUM USING FULL-FIELD MEASUREMENTS AT VARIOUS DEFORMATION RATES	26
CHAPTER 5: RELATIVE GRAIN SIZE COMPARISON STUDY	64
CHAPTER 6: SUMMARY AND RECOMMENDATIONS.....	73
BIBLIOGRAPHY	76

LIST OF FIGURES

Figure 3.1. Contour maps of the sample illustrating the evolution of the in-plane components ε_{xx} , ε_{yy} and ε_{xy} . The sample was loaded in the x-direction and the grain boundary lines are overlaid on the plots	20
Figure 3.2. Local rotation field evolution plot. Microstructural context is provided by a grain boundary overlay. Loading was applied in the x-direction	22
Figure 4.1. Schematic representation of the locations in a single Mg ingot from which samples were extracted. Loading directions are marked with bold arrows. Chill zones on the mold interior walls are not illustrated	32
Figure 4.2. (a) Optical micrograph showing the grain structure of a typical cast Mg specimen (sample 'E' in Figure 4.1). (b) speckled surface prepared for in-situ DIC.....	33
Figure 4.3. Quasi-static true stress-strain curves obtained for three different samples, shown on the right side of the plot	37
Figure 4.4. Evolution of intergranular cracking in quasi-static compression applied on a magnesium sample with microstructure shown in (a). Global compressive strain applied on the specimen are 6%, 8% and 12% in (b), (c) and (d), respectively. Location of the first visible cracks is magnified in (c). (e) DIC contour plot of the ε_{yy} component of the strain field taken at approximately 8% global strain where the mechanical failure is initiated (more on DIC in the later sections). Localized behavior of the deformation is concentrated at the boundary regions (Scale bar = 2 mm)	40
Figure 4.5. Dynamic true stress-strain curves of two measurements	43
Figure 4.6. Comparing global constitutive responses in quasi-static and dynamic loadings. Strain rate sensitivity, m , is determined as a function of strain using these curves	44
Figure 4.7. Contour maps showing the evolution of in-plane strain components at different global strain magnitudes for sample 'H'. Loading was applied in -y direction. Grain boundary outline is overlaid on contour maps	46
Figure 4.8. Schematic representation of mechanically relevant effective grain boundary thickness (EGBT) and grain interior (GI) regions in this work. Effective boundary thickness is denoted by δ_{GB}	49

Figure 4.9. Contour maps showing a highly heterogeneous distribution of (a) ϵ_{yy} and (b) ϵ_{xx} with a representative line segment ‘L’ used to determine EGBT. Variation of local strain components along L is shown in (c) and is used to determine δ_{GB} 50

Figure 4.10. Illustration of the methodology used to separate in-grain deformation from grain boundary region deformation. Solid green regions in each image indicates the DIC area of interest. Showing from left to right: Full-field DIC area of interest, in-grain DIC area of interest and grain boundary area of interest52

Figure 4.11. Variation of the parameter η with total strain for quasi-static samples. Symbols ‘H’, ‘V’ and ‘E’ indicate ‘Horizontal’, ‘Vertical’ and ‘Equiaxed’ grain orientations, respectively. See Figure 4.1 for more details.54

Figure 4.12. Variation of the parameter η with total strain for dynamic samples. Symbols ‘H’ and ‘V’ indicate ‘Horizontal’ and ‘Vertical’ grain orientations, respectively. See Figure 4.1 for more details55

Figure 4.13. η parameter data used for direct comparing of quasi-static and dynamic results. The data shown in this figure is for a sample with grains aligned perpendicular to the loading direction57

Figure 4.14 Ratio of η parameter for dynamic and quasi-static conditions versus total strain. ‘Dyn’ and ‘QS’ denote dynamic and quasi-static, respectively58

Figure 5.1. Indentation pattern in three corners to map an area of interest66

Figure 5.2. Full-field contour strain map of sample 1 featuring all three strain components shown by row. Columns represent the degree of global strain68

Figure 5.3. Sample 2 contour plots69

Figure 5.4. Contour strain maps of large grained magnesium sample tested under compression. This sample, in addition to the one featured in Figure 4.7 display a relatively homogenous grain size distribution70

LIST OF ABBREVIATIONS

DIC	Digital Image Correlation
EBSD	Electron Backscatter Diffraction
GBS	Grain Boundary Sliding
SPHB.....	Split Pressure Hopkinson Bar
TEM	Transmission Electron Microscopy

CHAPTER 1

INTRODUCTION

1.1 MATERIAL BEHAVIOR UNDER DYNAMIC CONDITIONS

For years it has been the goal of many efforts in the field of materials science and engineering to effectively characterize the consequences of subjecting solid materials to elevated strain rates. More specifically, the exact way a given material's deformation characteristics change under these conditions and how these changes are controlled has been a topic spanning the interest of numerous scientific communities. Understanding the mechanical response in this regard is crucial for designing a structure that will undergo potential shock or impact, or other environmental conditions that introduce dynamic stresses on a material. Exploring these phenomena is not only important to engineering design, but also in developing the complex models for future work in this field.

To date, there has been clear evidence in the literature to suggest that many common engineering parameters are rate-sensitive [1], meaning they take on different values in the dynamic regime as opposed to when they are subjected to just quasi-static loading; despite the material in question being identical in both cases.

In the mechanical sense, when a structure is deformed dynamically, the influence of high strain rates is known to dictate the amount and degree of the internal flow stress; which is known to initiate significant plastic wave propagation. This wave phenomenon can directly contribute to a wide range of material effects not seen in quasi-static testing [2-4]. In addition, this wave behavior can then be linked to the presence of adiabatic shear

banding generation commonly seen under dynamic loading [5]. Another unique feature of high strain rate deformation is the presence of significant inertia occurring within the material during an event. These inertia effects are the increase in momentum of the impacted portion of a specimen as it is propelled into the undeformed sections [6]. This inertia effect is known to cause noteworthy changes in the stress calculation for dynamic compression tests and is usually accounted for numerically using an integral form of a function [7].

All of the aforementioned dynamic effects can be observed in virtually all solid materials such as: polymers, foams, plastics and metals, however, more notable mechanical variabilities exist in metallic systems. For instance, much higher degrees of certain known deformation characteristics such as slip and twinning are achieved by applying high strain rates to a given material [8, 9]. Lastly, various other aspects of these deformation mechanisms in metals have been seen to change drastically depending on the applied strain rate which will be discussed thoroughly in the following chapter.

From a design standpoint, it is important to note that a given material's rate sensitivity may be dependent on multiple factors. For instance, some metals are known to display strain rate dependent limits with respect to its stress level and/or strain level [10]. Also, the size and general coarseness of the material grains influences the material's rate sensitivity [11-13]. The overall size of the material grains is also a central factor governing several other mechanical phenomena which will be covered in later sections.

1.2 CAPTURING DYNAMIC EVENTS

In modern experimentation, impact events are commonly generated by a Split Hopkinson Pressure Bar (SHPB) or some variant of this instrument. Analysis of the

dynamic response of materials for many years was limited to only examining the global response via extensometers and strain gauges. More recently, high speed imaging technology has allowed for high resolution recordings in real time, allowing for in-situ analysis. As a result, data can be extracted while the event is occurring, rather than strictly post-mortem. Depending on the spatial and temporal resolution, it is possible to visually dissect the deformation phenomenon as it occurs. However, the images themselves cannot quantitatively describe how the material in question deforms.

The technique of Digital Image Correlation (DIC) is known to effectively map the deformation evolution of various solid materials in-situ. DIC is a non-contact full-field strain measurement method that determines the in-plane deformation by analyzing images taken of the sample's surface as it deforms. When coupled with a high speed imaging system, DIC can provide high resolution data of a dynamic event.

DIC is the overarching method employed in all experimental works documented in this manuscript; the details of DIC operation specifics are beyond the scope of this work and will not be discussed but can be found elsewhere [14, 15].

1.3 STUDYING THE MICROSTRUCTURAL RESPONSE

In general, aptly mapping a material's microstructural behavior at sufficient resolution can prove challenging. In past works, the grain scale activity is usually described by using one or more of the following techniques: the global constitutive response characteristics, employing the use of Electron Backscatter Diffraction (EBSD) [16], or Transmission Electron Microscopy (TEM) [17]. These methods can clearly illustrate the misorientations and signs of certain deformation mechanisms in the microstructure and typical results from these applied methods will be discussed in the following chapter. These

tools are effective in accurately capturing local deformation mechanisms and texture evolution, however, they are unable to calculate the local strain occurring in the microstructure.

Recently, DIC analysis has been utilized to accurately describe the grain scale deformation behavior in several works [18, 19]. Yet, the extent to which DIC effectively quantifies local deformation at high resolution has not yet been fully tested in the dynamic regime.

1.4 OBJECTIVE

The present work seeks to validate a DIC-based method of characterizing the microstructural activity of a polycrystalline metal under both quasi-static and dynamic loading at sufficiently high resolution at multiple length scales. Pure magnesium is chosen for analysis in this regard and currently, there exists relatively few experimental works in the literature describing its localized deformation behavior at grain scales. As mentioned before, there have been a handful of previous efforts detailing the sharp contrast between high and low strain rate effects on pure magnesium. However, the in-situ dynamic material characteristics in the immediate presence of the grain boundaries at the meso-scale have yet to be fully examined.

The objective of this work is to present working high resolution full-field information regarding the regions in the microstructure most susceptible to damage and failure in both quasi-static and dynamic regimes. In addition, the experimental approach described in this manuscript attempts to draw conclusions regarding the locations and degree of likely deformation mechanisms suspected to be at work in a polycrystalline system; using magnesium as a case study.

1.5 LIST OF REFERENCES

- [1] Hutchinson JW, Neale KW. Influence of strain-rate sensitivity on necking under uniaxial tension. *Acta Metallurgica*. 1977. 25, 839-846.
- [2] Meyers M. *Dynamic behavior of materials* 1st ed. Wiley-interscience, New York, 1994. 1-4.
- [3] Malvern LE. Plastic wave propagation in a bar of material exhibiting a strain rate effect. *Quarterly of Applied Mathematics*. 1951. 8, 405-411
- [4] Ravindran S, Tessema A, Kidane A. Local deformation and failure mechanisms of polymer bonded energetic materials subjected to high strain rate loading. *Journal of Dynamic Behavior of Materials*. 2016. 2, 146-156.
- [5] Ravindran S, Tessema A, Kidane A. Multiscale damage evolution in polymer bonded sugar under dynamic loading. *Mechanics of Materials*. 2017. 114, 97-106.
- [6] Kappos AJ. *Dynamic loading design of structures*. Spon Press. New York, 2002.
- [7] Koohbor B, Kidane A, Lu W, Sutton MA. Investigation of the dynamic stress-strain response of compressible polymeric foam using a non-parametric analysis. *International Journal of Impact Engineering*. 2016. 91, 170-182.
- [8] Chichilia DR, Ramesha KT, Hemkera KJ. The high-strain rate response of alpha-titanium: experiments, deformation mechanisms and modeling. *Acta Materialia*. 1998. 46, 1025-1043.
- [9] Hazeli K, Kingstedt OT, Kannan V, Ravichandran G, Ramesh KT. Strain evolution and twinning modes in magnesium single crystal. Preprint submitted to Elsevier. 2016.
- [10] Weerasooriya, T. The MTL torsional split-Hopkinson bar. 1990. MTL-TR-90-27, U.S. Army
- [11] Wei Q, Cheng S, Ramesh KT, Ma E. Effect of nanocrystalline and ultrafine grain sizes on the strain rate sensitivity and activation volume: fcc versus bcc metals. *Materials Science and Engineering A*. 2004. 381, 71-79.
- [12] Schwaiger R, Moser B, Dao M, Chollacoop N, Suresh S. Some critical experiments on the strain-rate sensitivity of nanocrystalline nickel. *Acta Materialia*. 2003. 51, 5159-5172.
- [13] Wang YM, Ma E. Strain hardening, strain rate sensitivity, and ductility of nanostructured metals. *Materials Science and Engineering A*. 2004. 375-377, 46-52.

- [14] Sutton MA, Wolters WJ, Peters WH, Ranson WF, McNeill SR. Determination of displacements using an improved digital image correlation method. *Image and Vision Computing*. 1983. 1, 133-139.
- [15] Chu TC, Ranson WF, Sutton MA. Applications of digital-image-correlation techniques to experimental mechanics. *Experimental Mechanics*. 1985. 25, 232-244.
- [16] Humphreys FJ. Characterisation of fine-scale microstructures by electron backscatter diffraction (EBSD). *Scripta Materialia*. 2004. 51, 771-776.
- [17] Liu Q, Jensen J, Hansen N. Effect of grain orientation on deformation structure in cold-rolled polycrystalline aluminum. *Acta Materialia*. 1998. 46, 5819-5838.
- [18] Hong X, Godfrey A, Liu W, Orozco-Caballero A, Quinta da Fonseca J. Effect of pre-existing twinning on strain localization during deformation of a magnesium alloy. *Materials Letters*. 2017. doi: <http://d.doi.org/10.1016/j.matlet.2017.07.077>.
- [19] Ravindran S, Koohbor B, Kidane A. Experimental characterization of meso-scale deformation and the RVE size in plastically deformed carbon steel. *Wiley Strain*. 2016. E12217. doi: 10.1111/str.12217.

CHAPTER 2

OVERVIEW OF MAGNESIUM PROPERTIES

2.1 INTRODUCTION

In recent years, magnesium and its alloys have been used extensively in both aerospace and automotive applications [1] mainly due to its relatively high specific strength and inherent resistance to corrosion effects [2]. This corrosion resistance is also enhanced by exposing the material to heat treatment [3]. In general, the alloy forms typically consist of magnesium paired with other metals such as: aluminum, zinc or copper and are more commonly used in structures than pure magnesium. These metals are categorized as having a hexagonal closed-packed (hcp) crystal structure which features a limited number of active slip systems, making them experience more brittle type failure under sufficient load [4]. Despite this, a growing interest in utilizing magnesium in engineering applications exists, and the study of this material continues to be a subject of intrigue in the area of material science.

2.2 SYSTEM DEFORMATION CHARACTERISTICS

From an experimental perspective, it is critical to understand the main features of how magnesium structurally behaves under various conditions. Historically, several key deformation mechanisms are commonly detected under loading. Mechanical slip and twinning are the two main features observable during deformation, both of which can occur independently or in conjunction [5, 6]. Concerning the main differences between slip and twinning; the former is generally activated gradually as deformation progressively

increases, while twins nucleate abruptly in the lattice. Also, slip planes are smaller in width compared to twinning planes [7]. It should be noted that the mechanisms seen in magnesium are dependent on the ambient temperature; where slip and twinning are most commonly featured at temperatures below 473 K, whereas other mechanisms such as creep are seen at higher temperatures [8].

Of the five known slip systems and two twinning modes commonly associated with magnesium, the most common forms of each respective mechanism are prismatic and pyramidal slip modes; as well as $\{01\bar{1}2\}$ $\langle 01\bar{1}\bar{1}\rangle$ or extension twinning systems [5]. Extension twinning is activated upon the onset of plastic deformation, while compression twinning occurs in the latter stages and can relieve the accumulated stress concentrations in the material [9]. Additionally, extension or tension twinning is observed to be more prominent in the dynamic regime for hcp metals [10]. Furthermore, it was concluded by Dixit et al. [11] that the rapid development of microstructural twinning was the primary mechanism responsible for increased work hardening in dynamically deformed pure magnesium.

In a more general case, Molodov et al. [12], determined that as more modes of twinning are initiated in magnesium, a higher overall strain hardening rate is observed. Twinning has also been shown to be related to the specimen strain rate; under elevated strain rates twinning in magnesium was characterized by Hazeli et al. [13] who found that the number of twins that would form in the microstructure was greater and occurred at higher degrees of global strain when compared to the quasi-static regime, and that the observed twins only displayed a single orientation. Both of these findings were also observed by Dudamell, et al [14].

The nucleation of mechanical twinning is also known to be positively correlated with the size of the material grains [15]. This is also supported by a more extensive work done by Dobron et al. using acoustic emission techniques [16], which demonstrated that twinning nucleation is heavily favored in the larger grains at lower levels of global strain and is later initiated in smaller grains at higher levels of strain. However, this notion is somewhat challenged by a work done by Li, et al [17] who found that the onset of twinning plays a significant role even in smaller grains.

With regard to temperature effects on twinning, Chino et al. [18] made several notable observations in regards to the twinning behavior of a magnesium alloy: twin generation was suppressed when the material was exposed to higher temperatures and the texture is heavily correlated to the overall susceptibility to twin nucleation. This is also confirmed in a separate work by Tucker, et al [19] where twinning volume was shown to increase with applied strain rate, irrespective of rolling or transverse directions of a magnesium alloy.

The type and degree of grain boundary activity has also been studied extensively in the literature, mainly how much the regions in the area of grain boundaries contribute to the overall deformation of magnesium. Grain boundary triple junction points are known to be areas of more concentrated boundary action. Contrary to what is typically seen at a single boundary line, triple junctions experience additional rotations and varying sorts of grain boundary displacement under loading [20].

Grain Boundary Sliding (GBS) in polycrystalline metals is shown to cause cracks along the boundaries, particularly in the presence of triple junction points [21]. GBS is another commonly featured phenomenon in the area of grain boundary motion, and is also

suspected to be related to the amount of triple junction migration; a type of grain boundary motion that occurs during deformation [22]. Unlike some of the previously mentioned deformation mechanisms, GBS can be prominently featured at both low and high levels of strain, and is not strictly limited to a specific regime of magnesium's deformability [23].

In efforts to make the response of magnesium more predictable, a degree of control over some of the material behavior can be obtained via grain refinement, leading to several notable effects. One of these is increased amount of GBS seen occurring in the material. Koike et al, [24] reported a greater amount of GBS at room temperature and that the variant of GBS seen here is induced by slip at the grain boundaries. Secondly, it was concluded by Somekawa et al. that the refinement of the grains in pure magnesium led to an increase in its overall fracture toughness and yielding strength [25]. Lastly, grain refinement through plastic processes has been shown to increase the overall ductility of magnesium based alloys even at relatively low temperatures [4, 26, 27].

Several studies have documented the mechanical response of magnesium and its alloys specifically at elevated strain rates. More generally, the overall yield stress and shear modulus of magnesium is known to be sensitive to various parameters such as pressure and temperature effects; therefore this will influence the degree of work hardening seen in the dynamic case [28]. Later, Ishikawa, et al [29] observed that the primarily featured phenomena were dislocation glide and mechanical twinning regardless of the ambient temperature.

Another work by Li, et al [30], found that based on the shape of the stress-strain response of Mg alloy under dynamic compression, that twinning was a factor in its deformation. Evidence of twinning in a magnesium alloy was also documented in a

comprehensive study which detailed the effects of sample orientation on the twinning phenomenon. Several magnesium alloy samples were cut at different angles and tested dynamically, revealing that strain hardening and the yield stress were heavily dependent on the angle of cut from the extruded magnesium sheet, and that twinning was seen to occur at relatively low levels of global strain. [31], although texture effects are thought to be a significant factor in this regard.

In addition to the mechanisms seen in the dynamic regime, Watanabe, et al [32] discovered that the plastic limit of a magnesium alloy can be extended considerably under certain temperature conditions under high strain rates. Finally, an interesting comparison study by Mukai, et al [33], showed that when a ZK60 Mg alloy is subjected to dynamic tension, the yield stress of the material increases overall.

2.3 LIST OF REFERENCES

- [1] Mordike BL, Ebert T, Magnesium: Properties, applications, potential. *Materials Science and Engineering A*. 302 (2001) 37-45.
- [2] Shaw BA. Corrosion Resistance of Magnesium Alloys, *ASM Handbook*. 13A .2003. 692-696.
- [3] Zhou W, Shen T, Aung N. Effect of heat treatment on corrosion behavior of magnesium alloy AZ91D in simulated body fluid. *Corrosion Science*. 2010. 52, 1035-1041.
- [4] Arab SM, Akbarzadeh A. Effect of equal channel angular pressing process on the microstructure of AZ31 Mg alloy strip shaped specimens. *Journal of Magnesium and Alloys*. 2013. 1, 145-149.
- [5] Stycznski A, Hartig C, Bohlen J, Letzig D. Cold rolling textures in AZ31 wrought magnesium alloy. *Scripta Materialia*. 2004. 50, 943-947.
- [6] Chino Y, Kimura K, Mabuchi M. Twinning behavior and deformation mechanisms of extruded AZ31 Mg alloy. *Materials Science and Engineering A*. 2008. 486, 481-488.
- [7] Balogh L, Niezgoda SR, Kanjarla AK, Brown DW, Clausen B, Liu W, Tome CN. Spatially resolved in situ strain measurements from an interior twinned grain in bulk polycrystalline AZ31 alloy. *Acta Materialia*. 2013. 61, 3612-3620.
- [8] Galiyev A, Kaibyshev R, Gottstein G. Correlation of plastic deformation and dynamic recrystallization in magnesium alloy ZK60. *Acta Materialia*. 2001. 49, 1199-1207.
- [9] Koike J. Enhanced deformation mechanisms by anisotropic plasticity in polycrystalline Mg alloys at room temperature. *Metallurgical and Materials Transactions: Physical Metallurgy and Materials Science, A*. 2005. 36, 1689-1696.
- [10] Dixit N, Hazeli K, Ramesh KT. Twinning in magnesium under dynamic loading. *EPJ Web of Conferences*. 2015. 15, doi: 10.1051/epjconf/20159402018.
- [11] Dixit N, Xie KY, Hemker KJ, Ramesh KT. Microstructural evolution of pure magnesium under high strain rate loading. *Acta Materialia*. 2015. 87, 56-67.
- [12] Molodov KD, Al-Samman T, Molodov DA. On the diversity of the plastic response of magnesium in plane strain compression. *Materials Science and Engineering A*. 2016. 651, 63-68.
- [13] Hazeli K, Kingstedt OT, Kannan V, Ravichandran G, Ramesh KT. Strain evolution and twinning modes in magnesium single crystal. Preprint submitted to Elsevier. 2016.

- [14] Dudamell NV, Ulacia I, Galvez F, Yi S, Bohlen J, Letzig D, Hurtado I, Perez-Prado MT. Twinning and grain subdivision during dynamic deformation of a Mg AZ31 sheet alloy at room temperature. *Acta Materialia*. 2011. 59, 6949-6962.
- [15] Meyers MA, Vohringer O, Lubarda VA. The onset of twinning in metals: a constitutive description. *Acta Materialia*. 2001. 49, 4025-4039.
- [16] Dobron P, Chmelik F, Yi S, Parfenenko K, Letzig D, Bohlen J. Grain size effects on the deformation twinning in an extruded magnesium alloy tested in compression. *Scripta Materialia*. 2011. 65, 424-427.
- [17] Li B, Joshi SP, Almagri O, Ma Q, Ramesh KT, Mukai T. Rate-dependent hardening due to twinning in an ultrafine-grained magnesium alloy. *Acta Materialia*. 2012. 60, 1818-1826.
- [18] Chino Y, Kimura K, Hakamada M, Mabuchi M. Mechanical anisotropy due to twinning in an extruded AZ31 Mg alloy. *Materials Science and Engineering A*. 2008. 485, 311-317.
- [19] Tucker MT, Horstemeyer MF, Gullett PM, El Kadiri H, Whittington WR. Anisotropic effects on the strain rate dependence of a wrought magnesium alloy. *Scripta Materialia*. 2009. 60, 182-185.
- [20] Gutkin MY, Ovid'ko IA, Skiba NV. Crossover from grain boundary sliding to rotational deformation in nanocrystalline materials. *Acta Materialia*. 2003. 51, 4059-4071.
- [21] Shimokawa T, Nakatani A, Kitagawa H. Grain size dependence of the relationship between intergranular and intragranular deformation of nanocrystalline Al by molecular dynamics simulations. *Physical Review B*. 2005. 71, 224110.
- [22] Van Swygenhoven H, Derlet PM. Grain-boundary sliding in nanocrystalline fcc metals. *Physical Review B*. 2001. 64, 224105.
- [23] Panicker R, Chokshi AH, Mishra RK, Verma R, Krajewski PE. Microstructural evolution and grain boundary sliding in a superplastic magnesium AZ31 alloy. *Acta Materialia*. 2009. 57, 3683-3693.
- [24] Koike J, Ohyama R, Kobayashi T, Suzuki M, Maruyama K. Grain-boundary sliding in AZ31 magnesium alloys at room temperature to 523 K. *Materials Transactions*. 2003. 44, 445-451.
- [25] Somekawa H, Mukai T. Effect of grain refinement on fracture toughness in extruded pure magnesium. *Scripta Materialia*. 2005. 53, 1059-1064.

- [26] Li B, Joshi S, Azevedo K, Ma E, Ramesh KT, Figueiredo RB, Langdon TG. Dynamic testing at high strain rates of an ultrafine-grained magnesium alloy processed by ECAP. *Materials Science and Engineering A*. 2009. 517, 24-29.
- [27] Yamashita, A., Horita, Z., Langdon, T.G., 2001. Improving the mechanical properties of magnesium and a magnesium alloy through severe plastic deformation. *Materials Science and Engineering*. 300, 142-147.
- [28] Steinberg DJ, Cochran SG, Guinan MW. A constitutive model for metals applicable at high strain rate. *Journal of Applied Physics*. 1980. 51, 1498.
- [29] Ishikawa K, Watanabe H, Mukai T. High strain rate deformation behavior of an AZ91 magnesium alloy at elevated temperatures. *Materials Letters*. 2005. 59, 1511-1515.
- [30] Li B, Joshi S, Azevedo K, Ma E, Ramesh KT, Figueiredo RB, Langdon TG. Dynamic testing at high strain rates of an ultrafine-grained magnesium alloy processed by ECAP. *Materials Science and Engineering A*. 2009. 517, 24-29.
- [31] Yang Y, Wang F, Tan C, Wu Y, Cai H. Plastic deformation mechanisms of AZ31 magnesium alloy under high strain rate compression. *Transactions of Nonferrous Metals Society of China*. 2008. 18, 1043-1046.
- [32] Watanabe H, Mukai T, Ishikawa K, Higashi K. High-strain-rate superplasticity in an AZ91 magnesium alloy processed by ingot metallurgy route. *Materials Transactions*. 2002. 43, 78-80.
- [33] Mukai T, Yamanoi M, Watanabe H, Ishikawa K, Higashi K. Effect of grain refinement on tensile ductility in ZK60 magnesium alloy under dynamic loading. *Materials Transactions*. 2001. 42, 1177-1181.

CHAPTER 3

ON THE IN-SITU LOCALIZED DEFORMATION BEHAVIOR OF PURE MAGNESIUM UNDER DYNAMIC LOADING¹

¹ Malchow P, Ravindran S, Kidane A. In preparation.

3.1 ABSTRACT

Dynamic grain boundary region deformation of pure magnesium was investigated and verified by utilizing in-situ full field strain measurements obtained from Digital Image Correlation (DIC) techniques. This method was confirmed to effectively characterize the microstructural response at high magnification of an area of interest in the vicinity of multiple grain boundaries and triple junctions. The highly heterogeneous evolution of the material strain patterns was quantified and it was determined that the highest concentrations of the localized response were seen to occur primarily at the interfaces between the grains, while the amount of in-grain deformation, specifically in the larger grains was minimal by comparison. Additionally, the calculated local rotations in the material were also seen to take place preferentially at the boundaries and triple junctions. Locations of suspected active slip and twinning regions were identified and conclusions about other possible modes of deformation are discussed.

Keywords: Metals and alloys, microstructure, deformation and fracture, magnesium, high-strain rate, Digital Image Correlation

3.2 INTRODUCTION

Magnesium and its alloys have been implemented in many engineering branches, such as aerospace and automotive applications [1]. A primary reason for its increased use is that it possesses a high specific strength at room temperature along with an inherent resistance to corrosion [2]. However, magnesium is a low-ductility metal that exhibits weak grain boundaries under loading, which occurs as a result of the limited number of slip systems at room temperature [3]. This gives rise to a significant degree of the local deformation occurring in the regions of grain boundaries. Magnesium features a hexagonal

closed packed (hcp) crystal structure, consequently it shows increased formation of mechanical twins under plastic deformation [4].

The dominant deformation mechanisms in magnesium are prismatic and pyramidal slip modes, as well as $\{01\bar{1}2\} \langle 01\bar{1}\bar{1} \rangle$ twinning systems [5]; with the onset of twinning being positively correlated with grain size [6]. Under high strain rates, the number of twins in magnesium is greater and occurs at higher levels of global strain when compared to the quasi-static case [7].

In general, material strain rate sensitivity is related to the grain size and overall coarseness of the grains [8]. Additionally, polycrystalline metals exhibit different amounts of various deformation characteristics depending on the applied strain rate [9]; as twinning, basal slip, grain boundary sliding, creep and work hardening are all rate sensitive parameters [10].

With regard to deformation mechanisms in the regions of grain boundaries, Grain Boundary Sliding (GBS) is known to cause cracks along the boundaries particularly in the presence of triple junctions [11]. Triple junction points are associated with concentrated boundary action, and as opposed to a single boundary, they experience additional rotations and different modes of grain boundary motion as the dislocation slip tends to change direction when reaching a triple point [12]. GBS is also correlated with the amount of triple junction migration that occurs; which is a variant of grain boundary motion [13].

In light of all this, the ability to quantify the local dynamic deformation behavior and modes in pure magnesium becomes critically important for effectively including it into designs and other practices. This is the first work documenting the full-field in-situ

dynamic deformation response of polycrystalline pure magnesium. Conclusions on the suspected modes of deformation are discussed based on the calculated localized strain data.

3.3 EXPERIMENTAL METHODS

3.3.1 SAMPLE PREPARATION

Nominally pure (99.9%) as-cast magnesium was used in the present work. This cast magnesium exhibits sufficiently large grain sizes (~500-1000 μm) to enable meso-scale measurements. Additionally, the as-cast condition shows relatively weak grain boundaries; increasing the probability of observing grain boundary deformation modes. The weak boundary regions are a product of impurities which tend to collect at these areas.

A cubic sample ($12 \times 12 \times 12 \text{ mm}^3$) was cut from a cast ingot using a band saw and machined to its final dimensions using a milling instrument. The surface of the sample was polished using incremental grits of sandpaper and further detailed utilizing a range of aqueous alumina powders thereby eliminating scratches and defects. The purpose of polishing was to prepare the surface such that the microstructure would be clearly visible following chemical etching. The specimen was etched for 10 minutes in a solution consisting of 6g picric acid, 5mL acetic acid, 10mL water and 100mL ethanol.

To enable DIC measurements, a black and white uniform speckle pattern was then applied to the polished surface using white spray paint and black carbon powder. Note that for our purposes, the powder offers a finer speckle configuration at higher magnifications than traditional black paint. The powder particle size was approximately 10 μm ; sufficiently small to choose optimal subset sizes during image correlation, which in turn will yield more detailed data.

3.3.2 EXPERIMENTAL SETUP

A strain rate of approximately 1000/s was applied using a Split Hopkinson Pressure Bar apparatus, which consisted of 25 mm diameter stainless steel incident, transmitted and striker bars. The lengths of both the incident and transmitted bars was 1.82 m. The striker bar was housed inside of an inert helium gas gun and loading was initiated when the striker bar was propelled into the incident bar.

The sample was held in place between the incident and transmitted bars while illuminated by a Photogenic flash lamp. Strain gauges fastened on both the incident and transmitted bars were used to detect the impact signal as it traveled along the length of both bars. The strain gauges were connected to a signal amplifier which outputted to an oscilloscope that captured the impact waveform. This impact signal also initiated the triggering of the camera.

Imaging was performed using an ultra high-speed CCD camera (Shimadzu Hypervision HPV-X2, Hadland Imaging) at 500,000 frames per second with an exposure time of 1700 ns, and a total of 128 images were recorded. The oscilloscope trigger level and delay time of the camera were carefully selected to enable the most precise timing of the recording window for accurately capturing the event.

In order to verify the grain boundary activity with sufficient spatial resolution, a high magnification Navitar extension tube with a 0.75x magnification lens was utilized. The field of view in this case was approximately $4.2 \times 2.3 \text{ mm}^2$ with a spatial resolution of $10.65 \text{ }\mu\text{m}/\text{pixel}$. The images were post-processed using subset and step sizes of $9 \times 9 \text{ pixel}^2$ and 1 pixel respectively, with a filter size of 11.

3.4 RESULTS AND DISCUSSION

3.4.1 FULL-FIELD STRAIN DATA

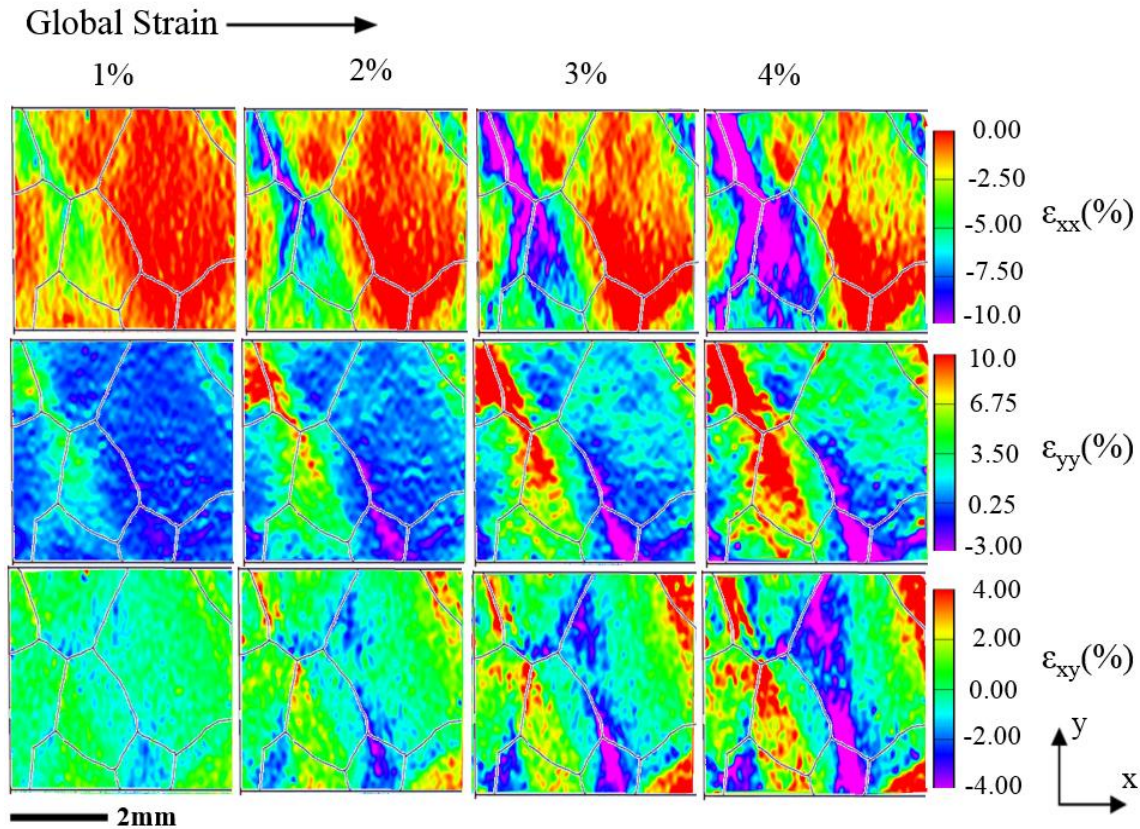


Figure 3.1. Contour maps of the sample illustrating the evolution of the in-plane components ϵ_{xx} , ϵ_{yy} and ϵ_{xy} . The sample was loaded in the x-direction and the grain boundary lines are overlaid on the plots.

Figure 3.1 displays the local full-field strain map and the microstructure is overlaid to provide context on the location of varying strain domains. The images are captured at approximately 1, 2, 3 and 4% global axial strain. Here, the strain localization along the grain boundaries is displayed by the large contrasts appearing close to the boundary lines. This phenomenon is particularly evident when examining the ϵ_{xx} and ϵ_{yy} components and this large variability in the normal components of strain is accompanied by the formation of shear deformations in the material.

From Figure 3.1, the localized strain values demonstrate a highly heterogeneous deformation pattern as certain regions exhibit higher magnitudes than the global strain. For instance, the local values in select regions of ε_{xx} and ε_{yy} are $\geq 10\%$ in the images of only 2% global strain.

Again, these concentrated areas are mainly located in the immediate vicinity of grain boundaries, as the highest values of ε_{xx} and ε_{yy} occur here and in the presence of triple junctions. Conversely, the amount of deformation activity taking place inside the larger grains remains minimal throughout the dynamic event. This concentration at the triple junctions is expected since damage nucleation is known to be more probable here than in single boundaries [14].

The high strain concentration around the boundaries coupled with a relatively low degree of intragranular deformation implies the main failure mechanism in this material is grain boundary cracking or intergranular fracture; (i.e. the grain boundaries are weak in comparison to the granular strength). This concentration of strain is most likely due to compatibility stresses which accumulate at interaction points between grains.

From a mechanical standpoint, DIC measurements are unable to distinguish specific deformation modes. Instead, DIC offers full-field information about the direct strain contribution of the suspected regions of these modes to the global strain. The highly localized areas which take place primarily inside the grains are believed to be a working combination of one or both of these mechanisms. This activity is especially clear when examining the ε_{yy} component, as there is a high degree of localization evident inside one of the smaller grains.

Figure 3.2 provides the full rotation field of material points occurring under dynamic loading at 1, 2, 3 and 4% axial strain. In general, it is known that large amounts of local rotation of the grains induces failure at the boundaries of a material [12].

3.4.2 LOCAL ROTATION FIELD

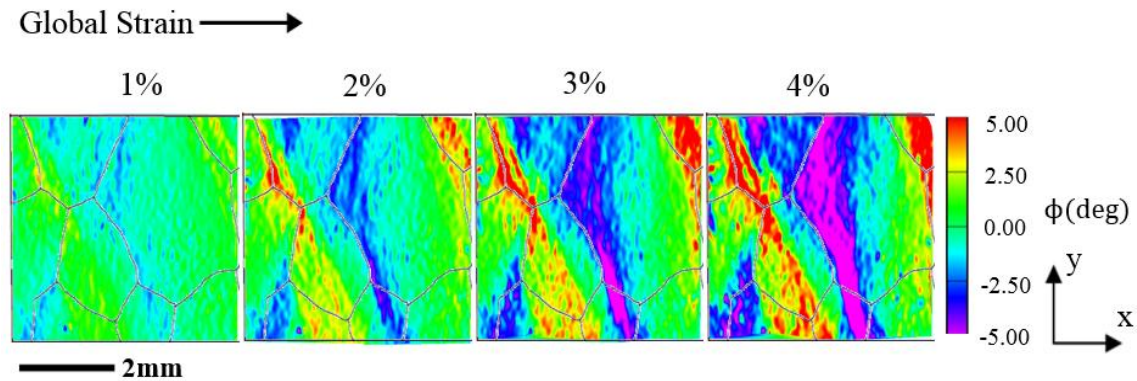


Figure 3.2. Local rotation evolution plot. Microstructural context is provided by a grain boundary overlay. Loading was applied in the x-direction.

In this experiment, a majority of the rotation takes place within the grains next to the boundaries, with some concentrations across the boundaries exclusively at triple junction points. The high values of $\phi \geq 5$ degrees are significant from one grain to another and once again shows that the grain boundary regions experience significant levels of localized activity. Moreover, the high amounts of rotation inside the larger grains compared to the boundaries imply a relatively unrestricted rotation, and the rotation at the triple junctions show a high degree occurring opposite the rotational direction of the larger adjacent grain.

3.5 CONCLUSION

The deformation of nominally pure magnesium was captured in-situ under high strain rate loading and analysis of the heterogeneous strain and rotation patterns across the microstructure was conducted using a DIC-based technique. Based on the observation of highly localized strain occurring at the grain boundaries particularly at triple junctions and

large rotation values within the grains, the boundaries in this material appear mechanically weak, while the larger grains are more resilient to in-grain deformation. Therefore, we conclude that the main mode of failure featured here is grain boundary fracture. Ultimately, this work demonstrates a unique methodology of applying DIC for effectively characterizing the microstructural response of a material at high strain rates. The details of this and related works regarding the behavior of polycrystalline metals provide insight into the mechanical factors governing its structural capabilities for future engineering practices and applications.

3.6 LIST OF REFERENCES

- [1] Hussein RO, Northwood DO. Improving the performance of magnesium alloys for automotive applications, *High Performance and Optimum Design of Structures and Materials*. 2014. 137, 1743-3509.
- [2] Shaw BA. Corrosion Resistance of Magnesium Alloys, *ASM Handbook*. 2003. 13A, 692-696.
- [3] Mordike BL, Ebert T. Magnesium: Properties, applications, potential. *Materials Science and Engineering A*. 2001. 302, 37-45.
- [4] Yoo MH, Morris JR, Ho KM, Agnew SR. Nonbasal Deformation Modes of HCP Metals and Alloys: Role of Dislocation Source and Mobility. *Metallurgical and Materials Transactions A*. 2002. 33A, 813-822.
- [5] Styczynski A, Hartig C, Bohlen J, Letzg D. Cold rolling texture in AZ31 wrought magnesium alloy. *Scripta Materialia*. 2004. 50, 943-947.
- [6] Meyers MA, Vohringer O, Lubarda VA. The onset of twinning in metals: a constitutive description. *Acta mater*. 2001. 49, 4025-4039.
- [7] Hazeli K, Kingstedt OT, Kannan V, Ravichandran G, Ramesh KT. Strain evolution and twinning modes in magnesium single crystal. Preprint submitted to Elsevier. 2016.
- [8] Wang YM, Ma E. Strain hardening, strain rate sensitivity, and ductility. *Materials Science and Engineering A*. 2004. 375–377, 46–52.
- [9] Dixit N, Xie KY, Hemker KJ, Ramesh KT. Microstructural evolution of pure magnesium under high strain rate loading. *Acta mater*. 2015. 87, 56-67.
- [10] Dixit N, Hazeli K, Ramesh KT. Twinning in magnesium under dynamic loading. *EPJ Web of Conferences*. 2015. 94, 02018.
- [11] Shimokawa T, Nakatani A, Kitagawa H. Grain size dependence of the relationship between inter and intra granular deformation of nanocrystalline Al by molecular dynamics. *Physical Review B*. 2005. 71, 224110.
- [12] Gutkin MY, Ovid'ko IA, Skiba NV. Crossover from grain boundary sliding to rotational deformation. *Acta mater*. 2003. 51, 4059-4071.
- [13] Van Swygenhoven H, Derlet PM. Grain boundary sliding in nanocrystalline fcc metals. *Physical Review B*. 2001. 64, 224105.
- [14] Bieler TR, et al. The role of heterogeneous deformation on damage nucleation at grain boundaries in single phase metals. *Int. J. Plast*. 2009. 25, 1655-1683.

[15] Ke M, Hackney SA, Milligan WW, Aifantis EC. Observation and measurement of grain rotation and plastic strain in nanostructured metal thin films. *Nanostructured Materials*. 1995. 5, 689-697.

CHAPTER 4

IN-SITU QUANTIFICATION OF INTRA AND INTERGRANULAR DEFORMATION IN PURE MAGNESIUM USING FULL-FIELD MEASUREMENTS AT VARIOUS DEFORMATION RATES²

² Malchow P, Koohbor B, Ravindran S, Kidane A. Submitted to *Int. J. Plast.*, 08/12/2017.

4.1 ABSTRACT

Owing to the presence of weak grain boundaries as well as significantly coarse grains with minimal deformability, grain boundary cracking is almost an inevitable source of failure when a cast magnesium-based alloy is to be deformed at relatively low temperatures. Our objective in this work is to quantitatively describe the contribution of inter- and intragranular deformation to the macroscale deformability and ductility of nominally pure as-cast magnesium subjected to quasi-static and dynamic loading. Our proposed meso-scale full-field approach is first presented and verified through measurements carried out to investigate deformation and grain boundary cracking in cast magnesium subjected to quasi-static loading. The same approach is then extended into analysis of meso-scale deformation and failure under dynamic loading conditions. A novel experimental setup consisting of a split Hopkinson pressure bar (SHPB) and a high-speed imaging system is used for in-situ quantification of deformation at microstructural levels under high strain rate loading conditions. Our results indicate that the contribution of grain boundary region deformation to the total strain applied on the Mg samples is significant and depends on the initial grain configuration. In addition, strain rate sensitivity of the material was found to be controlled to a higher degree by the grain boundary region deformation.

Keywords: A. ductility; B. constitutive behavior; B. rate-dependent material; C. Kolsky bar; digital image correlation

4.2 INTRODUCTION

The effects of grain boundaries on the properties of crystalline materials ranging from deformation resistance to electrical conductivity have been explored for decades.

From the mechanical behavior perspective, the presence of large fractions of grain boundaries (equivalent to having finer grains) is generally accepted to be associated with higher strength, higher fracture toughness and improved ductility [1]. However, certain metals and alloys may still show relatively low strength and brittle failure response, even with fine grain structures. Low strength grain boundaries and the delayed activation of slip systems in these polycrystalline metals are documented as being the principal sources for such mechanical behaviors [2].

Despite having a high specific strength and their growing applications in automotive and aerospace industries, magnesium and its alloys are among a group of materials which show low ductility at room temperature. This behavior is mainly due to limited activation of deformation systems at low working temperatures; while the activation of non-basal slip systems at elevated temperatures can significantly increase the degree of intragranular deformation, which in turn enhances the overall ductility of the material [3].

Although grain refinement through severe plastic deformation processes has been proven to increase the ductility of Mg-based alloys even at low working temperatures [4-6], these alloys are still generally regarded as low ductility materials. Without proper grain refinement, limited plastic deformation of Mg before failure is even more evident in as-cast conditions. In this regard, owing to the presence of weak grain boundaries, as well as significantly coarse grains with minimal deformability, grain boundary cracking is almost an inevitable cause of failure when a cast Mg-based alloy is to be deformed at relatively low temperatures.

Efforts have so far been devoted to studying intergranular fracture and nominally brittle behavior in various alloy systems, with particular attention given to materials with

hexagonal close packed (hcp) crystal structures. Among these are the work of Hughes et al. [2], in which a pseudo three-dimensional model consisting of hexagonal arrays was used to characterize cleavage cracking in polycrystalline zinc. Although such modeling approaches have proven to facilitate a more in-depth study of possible mechanisms governing deformation and failure in the examined materials systems, in-situ experimental observations to verify the modeling results are still very scarce. The lack of systematic experimental studies in this area may be due to challenges which arise with the implementation of high resolution in-situ measurement protocols that enable quantitative-based investigations, especially at grain scales.

Recent advances in the area of multi-scale full-field measurements, in particular the use of digital image correlation (DIC), have facilitated accurate quantification of inter- and intragranular deformation in a variety of material systems, from metals to polymer and ceramic composites [7-11]. The constant improvement of resolution in imaging devices has led to the enhancement of full-field deformation measurements at grain and sub-grain levels. Such improvements currently allow for studying grain-level in-situ strain localization and damage [12], slip band formation [13], micro-strain evolution in ultra-fine grained alloys [14], in-situ phase transformation [15], active slip system identification in polycrystalline metals [16-18], and parameter identification for crystal plasticity modeling and simulations [19, 20]. Despite constant improvements in spatial resolution of in-situ measurements carried out in slow deformation rates, research works dealing with in-situ observation and study of meso-scale deformation at high rates of strain is still very limited. To the best of our knowledge, there exists only a few studies that take into account in-situ dynamic deformation measurements in metallic systems [21].

Recent trends in the literature have seen growing interest in the applications of full-field measurements for in-situ investigations of local deformation and failure phenomena in a number of different material systems subjected to dynamic loading conditions [22-24]. Advances in high-speed and ultra-high speed cameras, in terms of both spatial and temporal resolutions [25] have provided the means for such studies.

Our objective in this work is to present our latest findings in meso-scale full-field measurements conducted on nominally pure cast magnesium to provide quantitative information on the ratio of inter- and intragranular strain as it relates to the macroscale material characteristics of deformability and ductility. Our proposed approach is first presented and verified through optical-based Digital Image Correlation (DIC) measurements carried out to investigate deformation and grain boundary cracking under quasi-static loading conditions. The same approach is then extended into the analysis of meso-scale deformation and failure for the dynamic case. To this end, a novel experimental setup consisting of a split Hopkinson pressure bar (SHPB) and a high-speed imaging system is used to enable in-situ quantification of deformation at microstructural levels under high strain rate loading conditions. Material responses under different strain rate conditions are compared and discussed in detail.

4.3 EXPERIMENTAL

4.3.1 MATERIAL AND SPECIMEN GEOMETRY

The material examined in this work was nominally pure (99.9%) as-cast magnesium. The reason for choosing the as-cast condition was supported by the facts that (1) grain structure in a cast magnesium ingot is coarse enough to enable optical-based meso-scale full-field measurements with proper resolution, (2) the grain boundaries here are

mechanically weak and therefore the probability of grain boundary cracking and intergranular fracture escalates, (3) a single ingot of cast magnesium can offer a wide variety of grain shapes and orientations. The latter point will be discussed in more details in the following sections.

Cubic samples ($10 \times 10 \times 10 \text{ mm}^3$) were cut from a single cast ingot using a band saw and machined using a milling apparatus. Samples for quasi-static conditions were extracted from various locations of the ingot to provide a range of different grain shape/orientations. Figure 4.1 schematically shows the locations from which quasi-static samples were extracted.

It should be noted that an as-cast magnesium ingot contains a wide range of grain structures. Due to the nature of solidification processes in pure metals, columnar grains are formed on the inner mold wall and are elongated towards the center of the ingot. A central zone containing equiaxed grains is also formed over the central zones.

Depending on the purpose, specimen location and loading directions can be selected such that a variety of different loading conditions and mechanical responses can be studied with respect to the initial grain configuration. Our samples were extracted such that the influence of grain orientation and loading direction is reflected in the measurements. In the present work, for simplicity, samples were named as ‘H’, ‘V’ and ‘E’, for horizontal, vertical and equiaxed grain configurations, respectively.

Common surface preparation practice, including stepwise grinding and polishing with an aqueous alumina powder mixture was applied for each sample. The relatively soft mechanical nature of cast magnesium made it difficult to achieve a mirror surface finish.

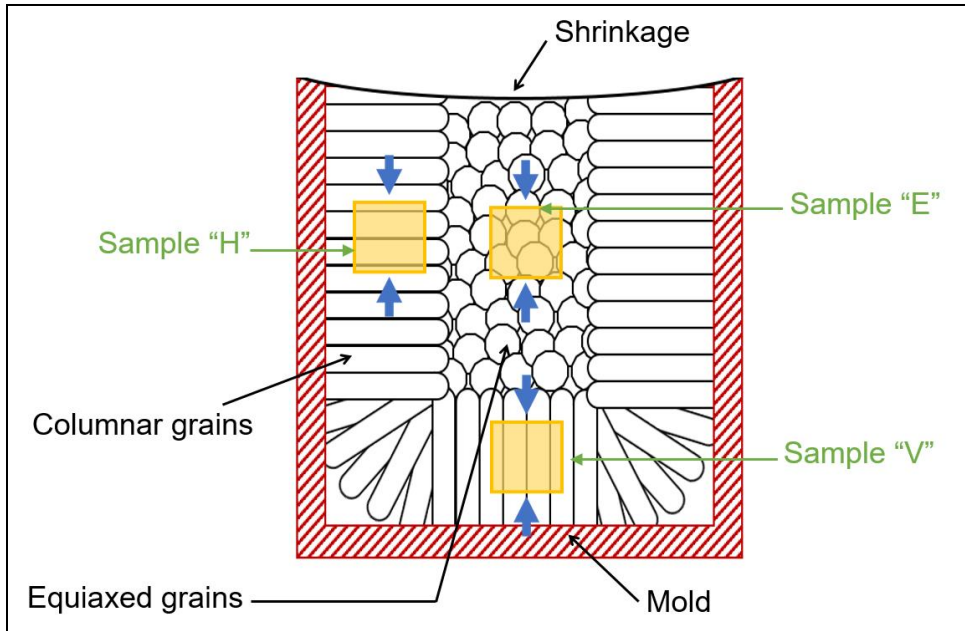


Figure 4.1. Schematic representation of the locations in a single Mg ingot from which samples were extracted. Loading directions are marked with bold arrows. Chill zones on the mold interior walls are not illustrated.

However, this was not considered to be a major issue in the present work because the sample surface was intentionally speckled to enable image correlation. Our main intention with polishing was to reveal the grain boundaries without the obstruction of major scratches or defects on the surface. The locations of these boundaries were later used to distinguish inter- and intragranular deformation domains. To reveal the microstructure, specimens were etched for 10 minutes in an etchant solution consisting of picric acid, acetic acid, water and ethanol. The typical microstructure of a magnesium sample in this work is depicted in Figure 4.2a. It should be stated that no notable impurity content was detected in the samples. The coarse millimeter-sized grain structure of the cast specimen is clearly shown in Figure 4.2a. One surface of each cubic sample was chosen to be speckled for full-field DIC measurements. Speckling was conducted in this work by first coating the sample surface with a thin layer of flat white paint.

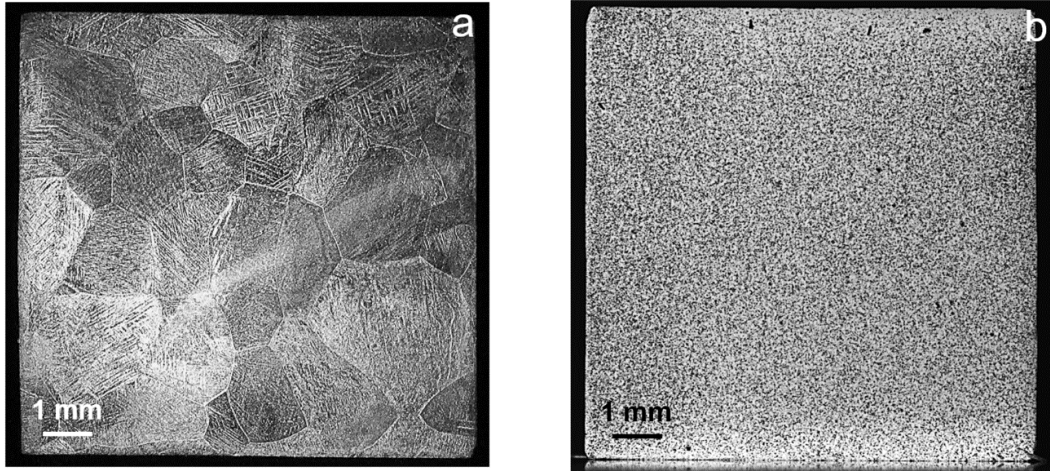


Figure 4.2. (a) Optical micrograph showing the grain structure of a typical cast Mg specimen (sample ‘E’ in Figure 4.1). (b) speckled surface prepared for in-situ DIC.

Immediately afterwards, a thin coat of black carbon powder was sprayed on the partially-dried white paint to produce a high-contrast and dense black and white pattern suitable for DIC measurements.

The average powder particle size in this work was 10 μm , small enough to enable the selection of a small correlation window (subset size) that allows for detection and study of highly localized deformation developed particularly in the vicinity of grain boundaries. Note that for our purposes, the carbon powder offers a much finer speckle configuration at higher magnifications than traditional black paint.

4.3.2 EXPERIMENTAL SETUP

Quasi-static experiments were carried out in a conventional compression testing machine with a 22 kN load-cell capacity. Measurement accuracy of the load-cell was ± 10 N, equivalent to ± 0.1 MPa margin of error in stress measurements. The specimen was placed between hardened stainless steel platens and compressed at a constant rate of 1 mm/min, equivalent to a nominal strain rate of 1.7×10^{-3} /s.

Images of the speckled surface during loading were acquired by a 5 MP CCD camera (Grasshopper GS3-U3-51S5M-C, FLIR) at a rate of 1 image per second and at a full-field resolution of 2448×2048 pixel². Imaging rate was synchronized with the load-cell sampling rate through the use of a data acquisition box, so that for each and every image acquired during loading, a corresponding load data point was also obtained. The camera was equipped with a 100 mm macro lens (Tokina) to enable high magnification imaging with minimal image distortion. Uniform lighting was provided by high intensity white LED lights.

Loading and imaging were continued until complete specimen failure. Images acquired during loading were then imported into the correlation software Vic-2D (Correlated Solutions, Inc.) for post-processing. Here, subset and step sizes of 33 pixels and 3 pixel were used, respectively. The strain filter size was selected to be 5, the smallest filter allowable in this software. Note that selecting these image correlation parameters was based on an extensive optimization process, details of which are beyond the scope of this work, but can be found elsewhere [26, 27]. In addition, the DIC parameters used in this work allow for investigating strong deformation gradients formed across grain boundaries.

Dynamic experiments were conducted in a conventional SHPB apparatus, consisting of 25 mm diameter stainless steel bars. Loading was initiated by a steel striker bar propelled by an inert helium gas gun. The length of both the incident and transmitted bars was 1.82 m, while the length of the striker bar was 0.45 m. To ensure yielding of the specimen, the necessary striker bar velocity was calculated to be approximately 11 m/s based on well-established SHPB equations [28]. The nominal strain rate applied on the specimen in the SHPB experiments was 1100 /s.

A single high-speed CCD camera (Fastcam SA-X2, Photron) was used to capture images of the dynamically deformed specimen during an approximately 500 μs event. The frame rate used was 100,000 frames per second.

The spatial resolution of the camera at the utilized frame rate was 384×260 pixel². For each experiment, the ends of the sample were lubricated and the specimen was held firmly between the incident and transmitted bars while illuminated by a Lumen 200 metal arc lamp. Lighting was kept only for several seconds to minimize heating effects.

Strain gauges on both the incident and transmitted bars were used to detect the impact signal. The strain gauges were connected to a signal amplifier which outputted to an oscilloscope that captured the impact waveform. This impact signal also initiated the triggering of the camera. Similar to our quasi-static experiments, images captured via high speed camera were processed initially using a subset size of 13×13 pixel², and a step size of 1 pixel with a filter size of 5. These DIC parameters allow for studying localized deformed domains with sufficient resolution.

Measurement performance, i.e. displacement and strain noise floors, for both quasi-static and dynamic camera systems were determined through a series of baseline measurements similar to the approach followed in Ref. [29].

Strain noise levels for quasi-static and dynamic experiments were found to be 945 $\mu\epsilon$ and 1530 $\mu\epsilon$, respectively. As a final note, due to negligible out-of-plane displacements as well as sufficiently high depth of field of the utilized imaging system, the influence of defocusing which resulted from out-of-plane motion was minimal.

4.4 RESULTS AND DISCUSSION

4.4.1 GLOBAL QUASI-STATIC STRESS-STRAIN RESPONSE

As previously described, a single ingot of cast magnesium may contain different grain structures. This is a consequence of the solidification process, a brief discussion of which was presented earlier. The presence of different grain shapes and configurations was taken advantage of in this work to explain the possible deformation and failure mechanisms that occurred in coarse-grained cast magnesium.

Quasi-static uniaxial compression was applied on specimens with different initial grain shapes and arrangements. Figure 4.3 shows the stress-strain curves obtained for three cubic specimens with different initial grain structures. Note that the global strain measurement in our quasi-static experiments was performed using the built in ‘virtual extensometer’ tool of the utilized DIC software, which provides highly accurate strain measurements with sub-pixel resolution. This being far more precise than the conventional compressive strain measurement based on platens displacement. This has been confirmed in the literature [24, 30].

In all cases, specimens show a nominally linear initial deformation, with nonlinear deformation initiating at approximately 35 MPa. This region is designated as ‘Region 1’, in which the slight differences between the curves are expected to be due to the initial arrangement and size of the grains. It should be emphasized here that depending on the crystallographic orientation of individual grains in each sample, some grains may start to plastically deform before the others [11]; however, the global yielding occurs when all grains start to deform plastically.

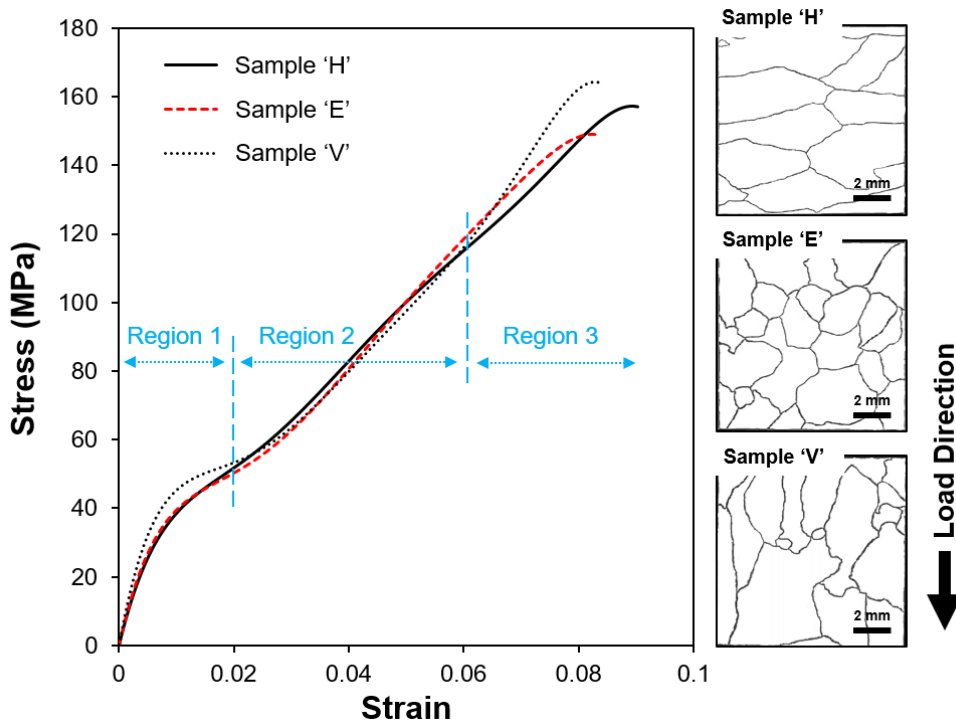


Figure 4.3. Quasi-static true stress-strain curves obtained for three different samples, shown on the right side of the plot.

After nominal yielding and upon entering Region 2, all curves converge and an arrangement-independent response is observed. Note that it is anticipated that the samples with different grain structures will show a different plastic deformation response; however, the deformation mechanisms for these samples might be such that a similar global mechanical response is obtained for our three samples; at least after the initial yielding. This behavior is explained through microstructural deformation measurements, discussed in detail in the forthcoming sections.

Upon further deformation and reaching Region 3, intergranular failure initiates in the form of cracks at grain boundaries and triple junctions, finally causing failure in the specimens. Figure 4.4 shows typical evolution of intergranular cracking and final failure in sample 'E'. Note that intergranular failure initiates from triple junctions (see figure 4.4).

Failure occurs at global compressive strains of approximately 8% in all cases. Specimen failure shows itself by formation of small visible cracks on the surface, as well as a drop in the global stress magnitude. The slight variations in the stress-strain curves may be due to the initial grain structure, as failure stress and strains differ slightly and also there are variations in region 1 for the specimens tested in this work. The possible reasons for this is discussed in the following sections.

Regardless of the configuration of the grains with respect to the loading direction, it was evidently shown that in quasi-static loading, failure always takes place by grain boundary fracture. This is indeed a well-understood phenomenon particularly for hcp metals, and is related to the role of grain boundaries in transferring in-grain cleavage from one grain to another [2]. In hcp metals, owing to insufficient active slip systems in low working temperatures, cleavage may happen in grains over some well-defined planes. Cleavage planes in neighboring grains do not necessarily meet in a line in their common grain boundary.

Therefore, the two cleavage planes within two neighboring planes intercept at the grain boundaries at some angle. Depending on the fracture resistance of the boundary, the mismatched strain resulting from the cleavage planes may be partially accommodated at the boundary. Previous studies have suggested that the deformation accommodation at grain boundaries significantly contributes to the overall failure strain of the material [31, 2]. Additionally, stress concentrated at grain boundaries suggests that the grains' configurations inherently make them more resistant to twinning activation [32].

However, the amount of such contributions has not been verified through in-situ experimental measurements. One particular objective in this work, as presented and

discussed in detail in the following, was to quantify the contribution of this grain boundary accommodation in the overall deformation of the examined material.

As a final remark in the study of global stress-strain response, our specimens in this work were deliberately machined to dimensions such that the study of grain scale deformations and grain interactions using an optical-based approach was possible. One may argue that a material with finer grains would have been readily used in high magnification optical (or electron) microscopies to conduct the same type of investigations. Although this would be a valid argument, our main intention in this work was to implement a systematic approach that can be used to facilitate studies in quasi-static as well as dynamic loadings. In dynamic loading, as discussed earlier in the introduction, high magnification full-field measurements are limited to optical-based approaches.

Due to this spatial resolution in dynamic conditions, full-field measurements are still substantially limited, therefore not allowing for high spatial and temporal resolution measurements.

4.4.2 GLOBAL DYNAMIC STRESS-STRAIN RESPONSE

Global dynamic stress-strain curves were obtained for the Mg specimens using a conventional SHPB apparatus. Figure 4.5 shows dynamic stress-strain curves obtained from two independent tests. The curves represent the constitutive response of samples with an initial grain structure similar to samples 'H' and 'V'; the two samples with the most different grain arrangements, in Figure 4.3. However, an accurate comparison between the dynamic stress-strain curves and those previously reported for Figure 4.3 cannot be made here.

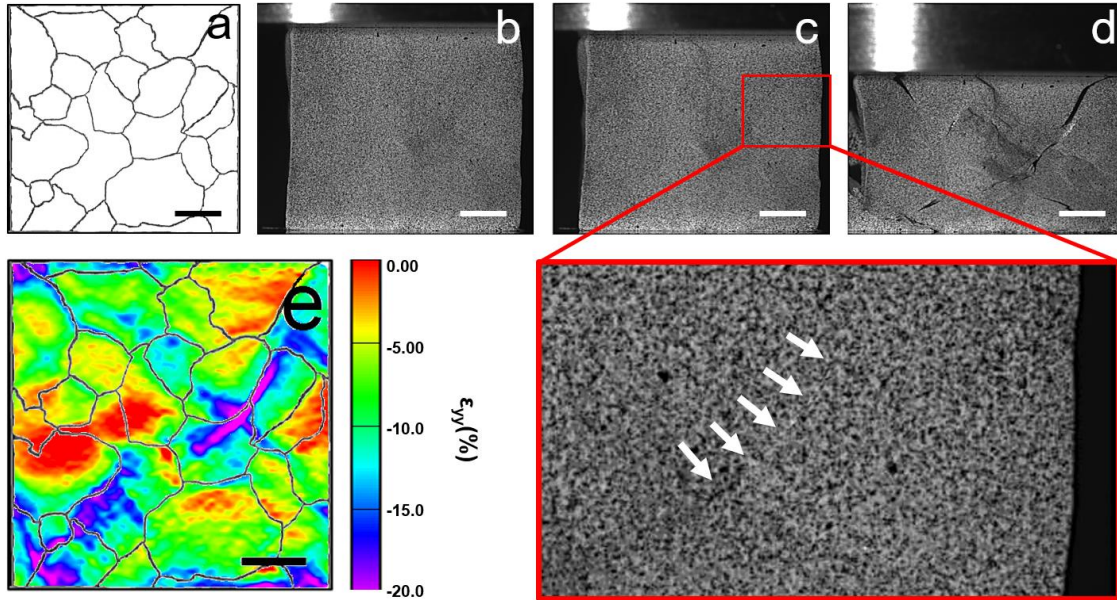


Figure 4.4. Evolution of intergranular cracking in quasi-static compression applied on a magnesium sample with microstructure shown in (a). Global compressive strain applied on the specimen are 6%, 8% and 12% in (b), (c) and (d), respectively. Location of the first visible cracks is magnified in (c). (e) DIC contour plot of the ε_{yy} component of the strain field taken at approximately 8% global strain where the mechanical failure is initiated (more on DIC in the later sections). Localized behavior of the deformation is concentrated at the boundary regions. (Scale bar = 2 mm).

This is clearly because in the quasi-static experiments, the applied load is directly measured by highly accurate load-cells, while in SHPB experiments, the stress is estimated from signals measured by the strain gauges and based on one-dimensional wave equations. (2) Depending on the material tested, the transient stress state may expand over several microseconds at the early stages of deformation [29, 33].

Such a behavior invalidates the stress measurements within the linearly elastic regime. Therefore, no conclusive remarks similar to those made for quasi-static experiments could be made here. Instead, a direct comparison between the stress-strain curves obtained in quasi-static and dynamic conditions has been made. Comparing quasi-static and dynamic stress-strain curves, the following remarks are highlighted:

1. Considering the general shape of the curves obtained from dynamic experiments, a downward concave appearance is exhibited. This shape is generally considered as an indication of higher work hardening rates, which in the particular case of Mg and its alloys, is related to the occurrence of higher amounts of twinning during deformation [34, 5]. Increased amounts of twinning leads to higher levels of work hardening, resulting in a noticeable concave shape in the stress-strain curve. Interestingly, the sample corresponding to Test 2 in Figure 4.5 had a similar structure to sample 'H' in Figure 4.3. For this sample, as most of the grains were oriented perpendicular with the loading direction, minimal shear strain was expected to develop on grain boundaries, and the applied global deformation was mostly consumed in deforming the grains, rather than shearing the boundaries.
2. Nominal failure strains achieved in dynamic loading are slightly higher than those in quasi-static experiments. This observation is consistent with previous ones [5], and is explained through remarkable twinning and dislocation activities in high strain rate compression of magnesium [35, 36].

Note that the formation of twins could not be observed and studied in this work, due to limitations in the spatial resolution of our full-field measurements. In particular, in-situ study of twinning in dynamic loading requires substantially higher resolutions and could not be achieved using the utilized imaging system. Apparent failed specimen characteristics here were similar to those observed in quasi-static experiments. This means that the fracture in this case was also observed to initiate from the boundaries and triple junctions in the material, leading to total failure.

However, in the case of dynamic loading, because of the limited control that can be applied on the experiment end, loading was continued until complete crushing and disintegration of the samples. The dynamic samples saw failure strains slightly higher than the quasi-static at around 9%.

Figure 4.6 compares the constitutive response of the material under two loading conditions. Curves representing quasi-static and dynamic response were the averages of those previously shown in Figures 4.3 and 4.5. The strain rate sensitivity parameter, m , was determined from these curves using the following simple definition:

$$m(\varepsilon) = \frac{\ln(\sigma_d/\sigma_s)}{\ln(\dot{\varepsilon}_d/\dot{\varepsilon}_s)} \quad (4.1)$$

where subscripts ‘d’ and ‘s’ denote dynamic and quasi-static, respectively, along with their true stresses and strains calculated previously.

The initial increase in the strain rate hardening is consistent with the observations made by Dixit et al. [35], and is due to a rapid increase of twins in the structure, which promote the overall work-hardening of the material subjected to dynamic deformation.

Strain rate sensitivity then reaches a maximum at a strain magnitude of *ca.* 2% and decreases afterwards. The rate of decreasing m with strain accelerates at strains > 6%, within a region that corresponds to Region 3 previously shown in Figure 4.3. The trend observed for the parameter m confirms that strain rate sensitivity of the material is indeed related to the microstructural aspects in the material.

Specifically, as the contribution of intergranular deformation becomes more prominent at higher global strains, the material is expected to become less strain rate sensitive.

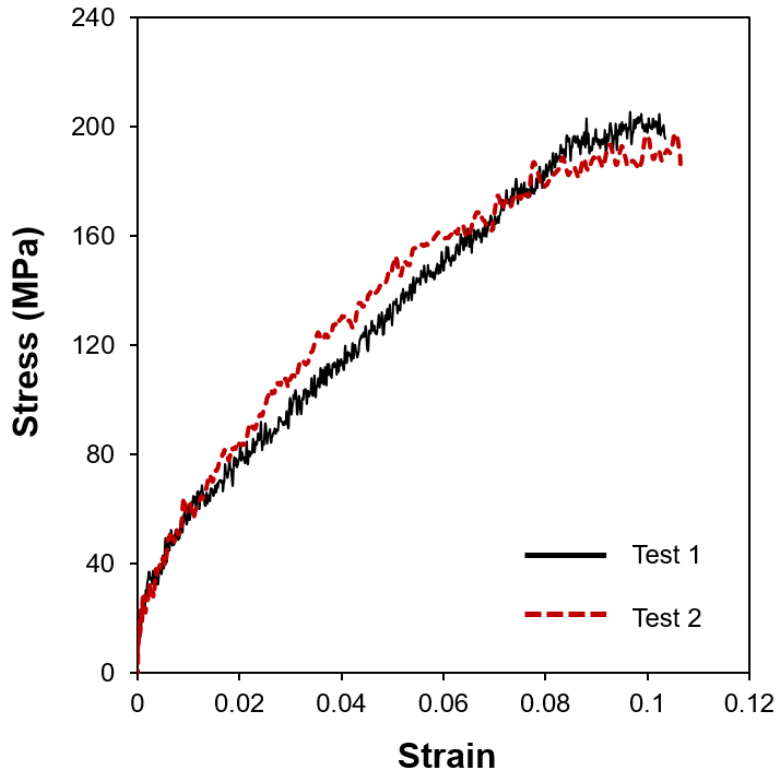


Figure 4.5. Dynamic true stress-strain curves of two measurements.

This further indicates that the two competing mechanisms described earlier, i.e. intra- and intergranular deformations, might show different strain rate sensitivities [37, 38]. Further elaborations and quantification in this regard are provided in the forthcoming sections where local strain maps are presented and discussed.

4.4.3. LOCAL STRAIN MAPPING AND POSSIBLE DEFORMATION MECHANISMS

The global stress-strain behavior of the samples indicated that there must be two principal mechanisms governing the overall deformation and failure of the cast magnesium. These two mechanisms are intra and intergranular deformation, the former was shown to be the dominant mechanism at lower global strains. Intergranular, or grain boundary region deformation, on the other hand, was described as the major deformation mechanism controlling deformation and failure at grain boundaries, becoming more

significant at larger nominal strains and characterized as being less sensitive to the applied strain rate.

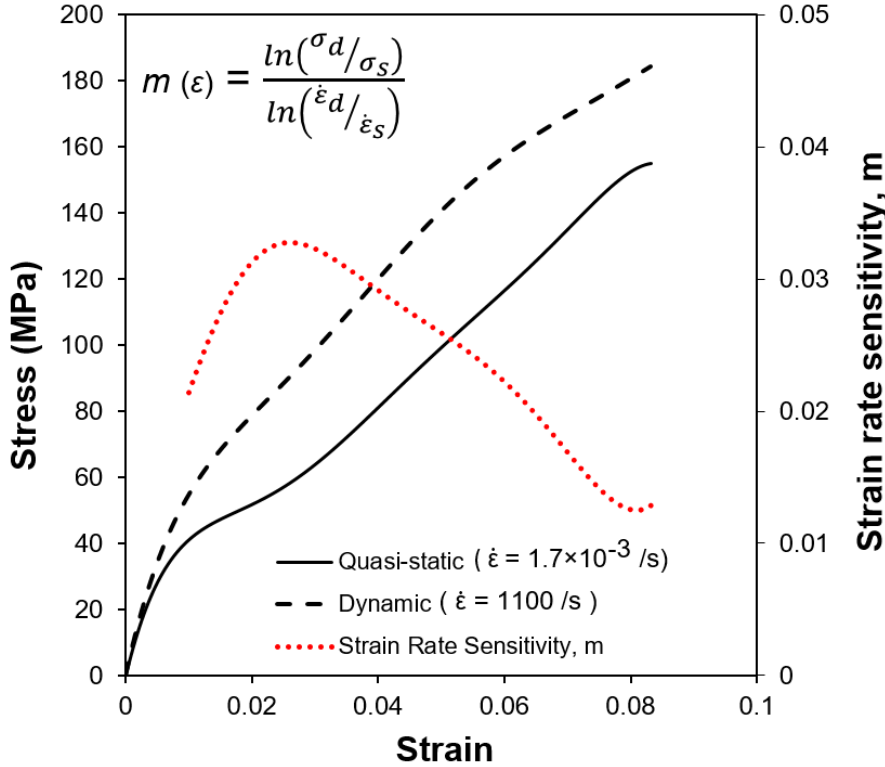


Figure 4.6. Comparing global constitutive responses in quasi-static and dynamic loadings. Strain rate sensitivity, m , is determined as a function of strain using these curves.

In order to provide more quantitative evidence on these competing mechanisms, we will hereafter focus on our full-field measurement data. Figure 4.7 shows typical local strain maps obtained for sample ‘H’ (see Figures 4.1 and 4.3) under quasi-static loading conditions. Initial grain boundaries are overlaid on strain maps in order to give an insight on the location of high and low strain domains. In Figure 4.7, the columns represent the images at approximately 1, 2, 3 and 4% global strain. From these images, the strain localization between the grain boundaries is evidenced by the large contrasts along and across the grain boundary overlay. This is especially clear when analyzing the ϵ_{yy} and ϵ_{xx}

maps. Here, as the evolution of the strain progresses, the horizontal alignment of the grains and the initialization of grain boundary sliding (GBS) is evident. Even if the overlay was never utilized, the grain boundaries would appear clearly in the contour maps. Substantial variabilities in the local normal components of strain is accommodated by the formation of strong shear deformations in the material, as evidently shown in Figure 4.7.

It is clearly observed that in-grain and grain boundary deformations show very different values than the global strains applied. The visibly wavy patterns is a result of the highly heterogeneous strain behavior. For instance, when examining the ϵ_{yy} component the large bands of red indicate that little to no localized deformation is occurring there, in contrast to the purple and pink regions which represent high magnitude strain behavior. A similar response was consistently seen in all specimens in this work. In addition, since we observe mechanical failure initiation at approximately 8% global strain, the full field information of the both the quasi-static and dynamic experiments showed clear shear banding occurring particularly when looking at the ϵ_{yy} component of the contour images.

It is interesting to note that the locally-developed strains can take significantly higher values than those applied globally. For instance, the ϵ_{yy} contour map shown in the upper right corner of Figure 4.7, corresponding to a 4% global strain exhibits areas that contain strains up to twice as high as that applied globally. It is more interesting to note that the nominal failure strain of the material in both quasi-static and dynamic loadings is below 10%, while local strain maps indicate substantially higher in-grain strains.

A reason for such a phenomenon might be that in spite of the hexagonal closed packed crystal structure of pure Mg, relatively small c/a ratios ($=1.622$) give rise to the activation of slip modes other than merely the basal slip system. In particular, prismatic

and pyramidal slip modes as well as $\{01\bar{1}2\} \langle 01\bar{1}\bar{1} \rangle$ twinning systems have also been identified to be active deformation modes in pure magnesium [39].

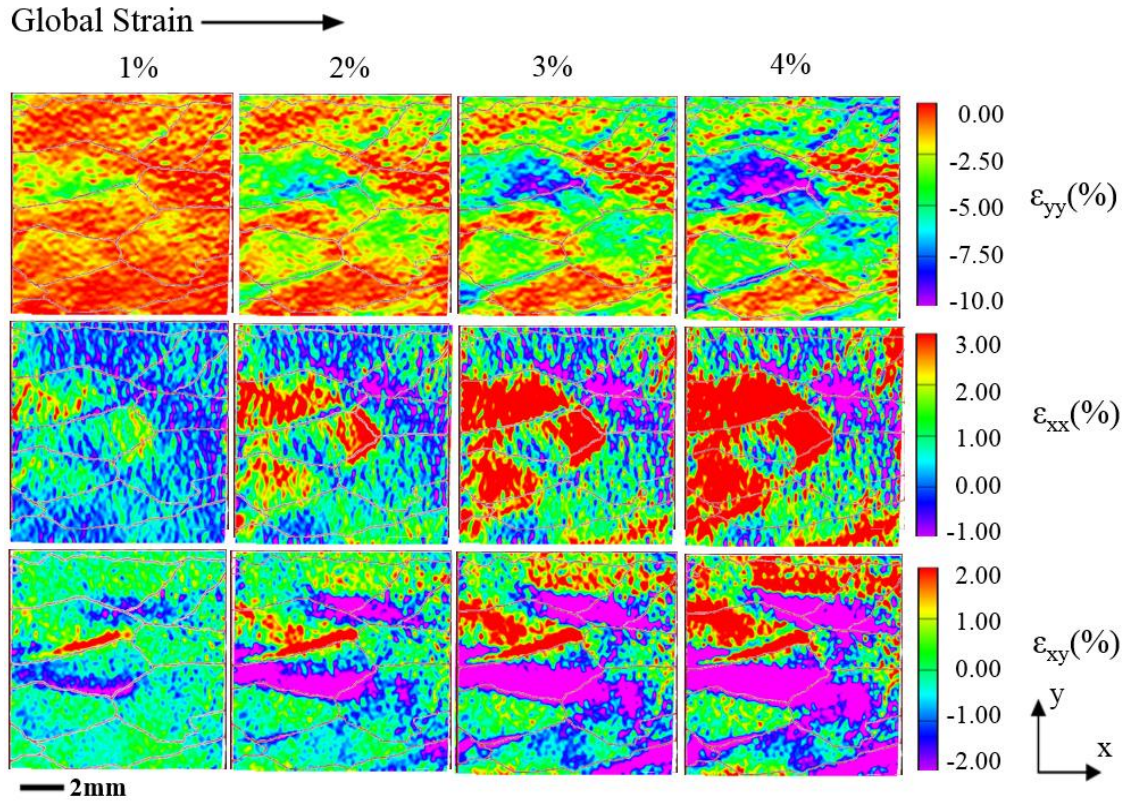


Figure 4.7. Contour maps showing the evolution of in-plane strain components at different global strain magnitudes for sample ‘H’. Loading was applied in -y direction. Grain boundary outline is overlaid on contour maps.

These modes can all contribute to the relatively large in-gain strain development in the material, also proving that low global failure strain is essentially controlled by limited deformation and failure resistance of grain boundaries. Of course, this explanation may not be generalized to all Mg alloys, since alloying elements are established to be capable of substantially altering the c/a ratio in magnesium [40]. With regard to our observations in the current work, the deformation activity occurring within the grains may be a working combination of some or all of the aforementioned mechanisms (see Fig 4.7). In addition,

the high concentration of strain occurring preferentially at the boundaries in our experiments indicates that these particular grains' arrangements lend themselves to be more resistant to twinning activation [32].

Furthermore, it is suspected in the early stages of deformation that grain boundary sliding is initiated because of the large differences in localized strain shown in the form of heavy contrasts in the contour plot, existing at the boundaries. Finally, this grain boundary activity ultimately leads to failure in the form of grain boundary fracture.

4.4.4 QUANTIFICATION OF IN-GRAIN AND GRAIN BOUNDARY DEFORMATION

Although strong deformation heterogeneities are clearly evidenced in the strain contours, full-field DIC measurements do not make a distinction between data obtained inside grains and that over the boundaries. Distinguishing in-grain deformation from that developed over the boundaries is an essential task in the present work, as we intend to quantify the contribution of each to the total strain applied on the samples. Therefore, we propose a simple approach in which we introduce a mechanically relevant 'effective grain boundary thickness (EGBT)' parameter to distinguish between deformation of the grain boundary regions and deformation developed at grain interiors.

Our proposed idea of EGBT is schematically shown in Figure 4.8. Note that the mechanically relevant effective boundary thickness introduced in this work is different from grain boundary width used for diffusion studies [41]. The concept used in diffusion studies considers a very narrow region typically with dimensions of a few nanometers used to characterize mass transfer through grain boundaries.

The notion of EGBT proposed in the present work is significantly larger in size, several orders of magnitudes larger than those used in diffusion studies. In addition, EGBT

is not an inherent material property, rather it depends mainly on the dimensions of the area of interest in a DIC-based measurement, and is highly sensitive to image correlation parameters used in a DIC analysis. In particular, image correlation parameters that facilitate measuring more localized deformation patterns at higher spatial resolutions allow for selecting thinner EGBTs. For more detailed discussions regarding the influence of image correlation parameters in measuring meso-scale deformation over highly localized regions refer to references [26, 27].

In order to quantify the EGBT in this work, local strain profiles across grain boundaries were considered. Figure 4.9 shows a typical evolution of in-plane strain components across a short representative line 'L'.

Local strain data over the representative line segment 'L' were plotted and fitted with proper Gaussian-type curves, as shown in Figure 4.9c. Gaussian curve fitting in this work was conducted in MATLAB®. Once the experimental data was fitted with the proper Gaussian function, the arithmetic mean and standard deviation were identified, and a one standard deviation span of the data was taken as the thickness of the effective grain boundary (δ_{GB}).

Due to higher accuracy and better spatial resolution of quasi-static measurements in this work, EGBT measurements were carried out for quasi-static specimens and the obtained values were used for the case of dynamic loading conditions as well. The above-mentioned approach was carried out several times for multiple line segments at various specimen locations. The average of all δ_{GB} measurements was obtained as 200 μm and was taken as the effective boundary thickness.

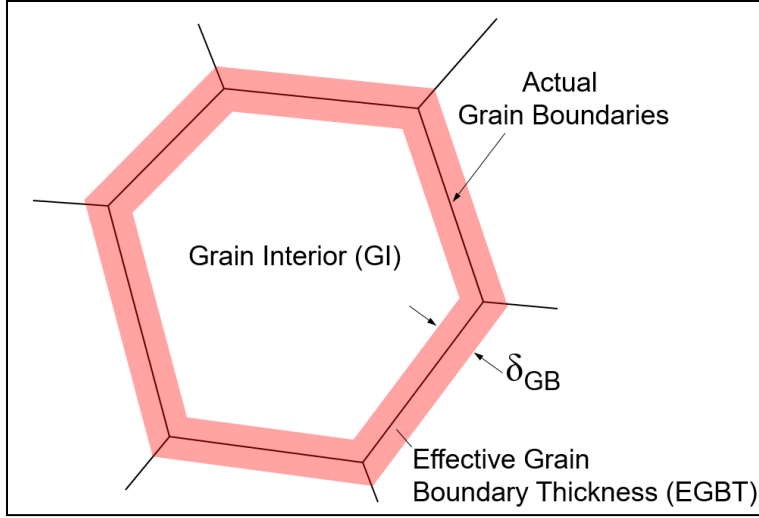


Figure 4.8. Schematic representation of mechanically relevant effective grain boundary thickness (EGBT) and grain interior (GI) regions in this work. Effective boundary thickness is denoted by δ_{GB} .

Next, strain evolutions over grain boundaries and grain interiors are considered and analyzed, in order to estimate the contribution of each mechanism to the total strain. Our methodology will be analogous to that proposed by Langdon [42]. In this approach, the total strain applied on the specimen, ε_T , may be expressed as:

$$\varepsilon_T = \varepsilon_{GI} + \varepsilon_{GB} \quad (4.2)$$

Where ε_{GI} is the strain associated with just the intragranular (in-grain) deformation, and ε_{GB} is the strain developed over the entire network of grain boundaries. Notice that the latter, i.e. ‘grain boundary strain’ henceforward refers to the strain developed over narrow effective grain boundaries, the thickness of which was determined as $\delta_{GB} = 200 \mu\text{m}$.

The contribution of grain boundary strains to the total strain, η , is then expressed as:

$$\eta = \frac{\varepsilon_{GB}}{\varepsilon_T} \quad (4.3)$$

whereas $(1 - \eta)$ indicates the contribution of in-grain strains to the total strain applied.

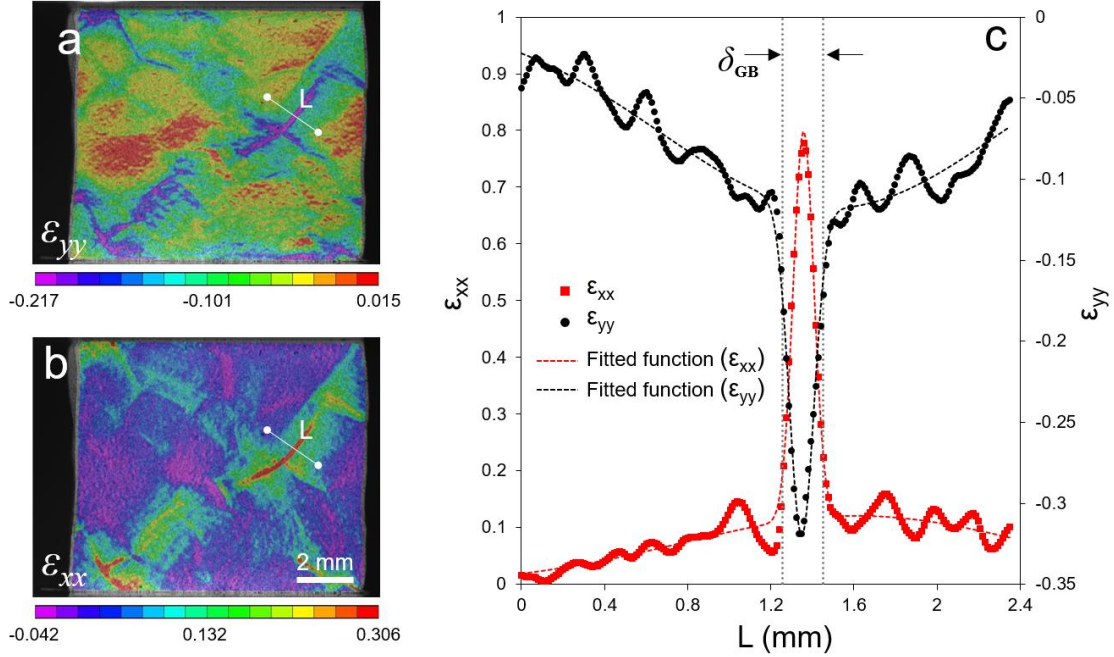


Figure 4.9. Contour maps showing a highly heterogeneous distribution of (a) ϵ_{yy} and (b) ϵ_{xx} with a representative line segment ‘L’ used to determine EGBT. Variation of local strain components along L is shown in (c) and is used to determine δ_{GB} .

Furthermore, due to the complex in-plane strain states, in order to enable a direct comparison of local and global strains, the definition of equivalent von Mises strain, ϵ^{eq} , is used to determine both in-grain and grain boundary strains. Equivalent strain in this regard is calculated as:

$$\epsilon_i^{eq} = \left[\frac{2}{3} (\epsilon_{xx}^2 + \epsilon_{yy}^2 + 2\epsilon_{xy}^2) \right]^{1/2} \quad (i: \text{‘GI’ or ‘GB’}) \quad (4.4)$$

From a practical point of view, separation of in-grain and grain boundary regions within a whole-field area of interest is cumbersome. To accomplish this task at higher accuracy levels, we carried out two separate image correlations for each sample. As shown in Figure 4.10, first, the whole speckled area was selected as the area of interest and all strain components were determined. Next, image correlation was performed again, this time with the initial area of interest only containing the grain interiors, from which the

effective grain boundaries were separated from the beginning. Finally, the strain data for just the grain boundaries was calculated using equation 4.2. Digital Image Correlation for strictly the grain boundary regions was not possible due to the areas of interest being far too narrow. Image correlation parameters (subset, step and strain filter) were chosen to be the same for all DIC runs. Again this approach is not rigorous and provides just a broad generalization about deformation activity occurring in the regions of the grain boundaries. Finally, all strain components were spatially averaged over the corresponding area of interest and further analyses were performed.

Figure 4.11 shows the variation of the parameter η with respect to the total strain applied on our quasi-static samples. All samples show significant variations in the value of η at strains lower than 0.02. This strain range is consistent with Region 1 discussed earlier in Figure 4.3, and is associated with the initiation of plastic deformation in the material, the occurrence of which is highly heterogeneous due to the initial Schmidt factor of the grains.

After plastic yielding, the η parameter takes on values close to 55% for sample 'H'. This indicates that the contribution of in-grain and deformation of the grain boundary regions is almost the same in the deformation of the sample with grains mostly oriented perpendicular to the loading direction. In sample 'V', the one with grain boundaries mostly aligned with the direction of the far-field load, the η factor displays higher values than those of sample 'H'.

This observation is indeed consistent with our previous discussions, and can be attributed to the occurrence of large local shear strains within the grain boundary network. The η parameter for this sample takes on values close to 0.7.

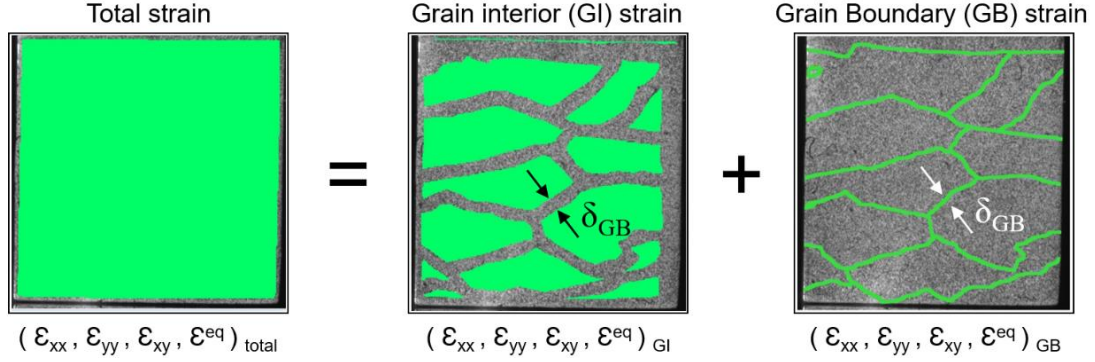


Figure 4.10. Illustration of the methodology used to separate in-grain deformation from grain boundary region deformation. Solid green regions in each image indicates the DIC area of interest. Showing from left to right: Full-field DIC area of interest, in-grain DIC area of interest and grain boundary area of interest.

Finally, in sample ‘E’, i.e., the sample with equiaxed grain arrangement, here the highest values of the η parameter are achieved. However, this behavior can be related to the comparably larger fraction of grain boundaries in this sample, which can accommodate higher local deformations in the areas more closely associated with grain boundaries for this sample. As a result, if we consider the high values of η as a percentage of the grain boundary regions for Sample ‘E’, then we would expect to see less extreme values, closer to Samples ‘V’ and ‘N’ after passing into Region 2. Because of this, our analysis will be primarily focused on the samples with ‘H’ and ‘V’ orientations for comparison purposes.

Interestingly, for all samples a slight change takes place at total strain values close to 0.05. This strain value is approximately at the transition strain between Regions 2 and 3 in Figure 4.3. Due to the unavailability of deformation data within the bulk of the samples, no further discussion can be provided on whether or not any internal damage in the form of grain boundary cracking occurred in the material. However, this can be a subject of interest for future computational studies or those facilitated by the use of X-ray tomography and volumetric image correlation [43, 44]. Regardless, our experimental measurements indicated that the role of grain boundaries in accommodating the deformation applied

quasi-statically on pure magnesium is substantial. The contribution of grain boundaries in this regard was quantified to be at least 50%. This value is higher than that previously obtained through computational approaches [2], and can be verified through more accurate and realistic crystal plasticity and micromechanics modelings in the future, which may utilize a more rigorous definition of the grain boundary regions.

Of course, one should bear in mind that the measurements in this work were limited to a single material. However, a similar approach can be implemented to study other HCP metals with more regular grain structures and mechanically stronger grain boundaries.

Similar to the approach used to identify the η parameter in quasi-static loading, this parameter was obtained for dynamic experiments as well. Figure 4.12 shows the variation of this parameter with respect to total strain applied on the samples in the SHPB experiments. Note that the strain rate in this case is approximately 1100/s and that the number of data points is significantly smaller, due to limited temporal resolution of the imaging in our dynamic experiments.

The general trends of the η parameter in dynamic experiments are similar to the quasi-static data, with the only difference being the value of the parameter η , which is significantly smaller in the dynamic experiments compared with the quasi-static tests. Results presented in Figure 4.12 indicate that in high strain rate experiments, the maximum contribution of grain boundaries to the overall deformation of the samples is approximately 40%, noticeably less than the values obtained for quasi-static conditions for the perpendicular and parallel oriented samples. Additionally, region 1 shows high levels of variability, which may be correlated with the fluctuation of the rate sensitivity in Figure 4.6.

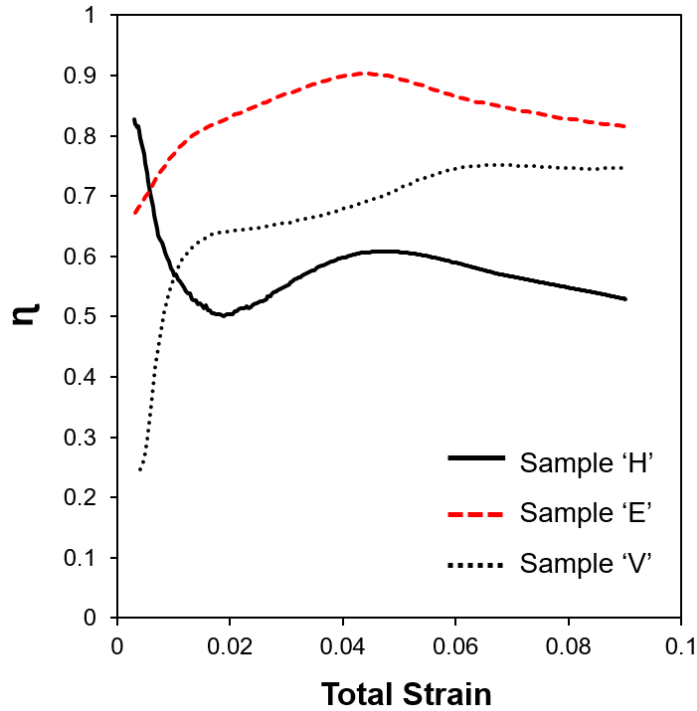


Figure 4.11. Variation of the parameter η with total strain for quasi-static samples. Symbols 'H', 'V' and 'E' indicate 'Horizontal', 'Vertical' and 'Equiaxed' grain configurations, respectively. See Figure 4.1 for more details.

Finally, in order to enable a quantitative assessment of the role of initial grain alignment on the contribution of grain boundary strain to the total deformation, quasi-static and dynamic η values were directly compared. Note that the direct comparison of the η data for quasi-static and dynamic loading conditions requires the same number of data points, and this was indeed a limiting point in our experiments, due to the considerably different experiment and interframe times.

To remedy this, η curves obtained for quasi-static and dynamic cases were first fitted with 6th degree polynomials, as typically shown in Figure 4.13. The curves were regenerated using the fitted polynomials and comparisons were made. Figure 4.14 compares the η parameter by showing the ratio of this parameter for dynamic loading over that of quasi-static experiments.

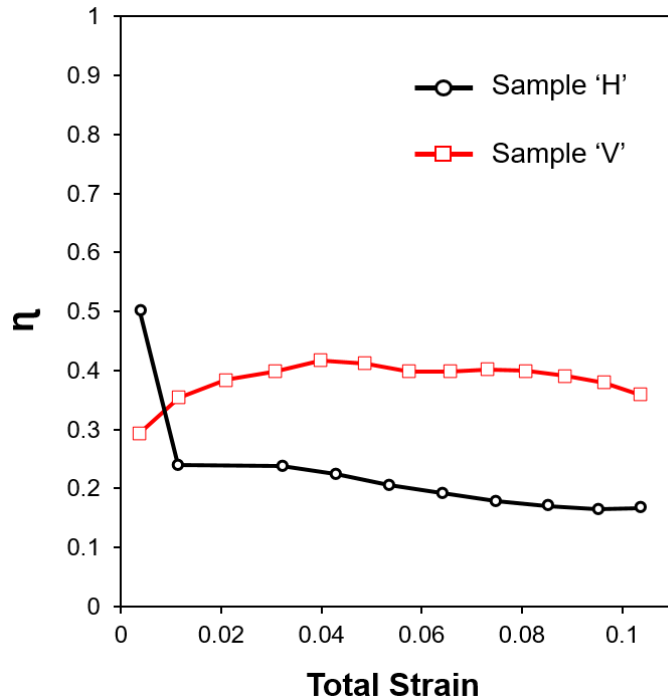


Figure 4.12. Variation of the parameter η with total strain for dynamic samples. Symbols 'H' and 'V' indicate 'Horizontal' and 'Vertical' grain orientations, respectively. See Figure 4.1 for more details.

Results are shown for both samples 'H' and 'V', i.e. those with grains elongated perpendicular and parallel to the loading direction, respectively. The following remarks are worth noting: (1) Contribution of the deformation of grain boundary regions to the total applied strain is more prominent for the sample with grains elongated parallel to the global loading direction, i.e. sample 'V'.

This is in fact anticipated and attributed to the more substantial shear deformation process. (2) After yielding, i.e. in Region 2, the relative difference between the η values decreases constantly with applied strain. This means that the contribution of grain boundary region deformation in dynamic loading gradually decreases compared with quasi-static loading conditions. Comparing the grain boundary strain with the strain rate sensitivity (m) data shown earlier in Figure 4.6, a consistent trend between the η -ratio and m can be found.

Considering this along with the data shown in Figure 4.13, it can be concluded that the deformation of the grain boundary regions plays a more significant role in the overall strain rate sensitivity of the material.

At large strain magnitudes applied dynamically, the overall deformation of the material is controlled to a larger extent by the in-grain deformation mechanisms rather than that the shear-dominated grain boundary deformation mechanisms. On the other hand, relatively higher strain rate sensitivity of the material at smaller total strains can be related with grain boundary region deformation mechanisms.

Our concluding statements above may be of particular significance in modeling works that tend to study deformation and failure response of brittle polycrystalline systems. In this regard, appropriate models accounting for the strain rate dependence of grain-boundary deformation seem to be essential in order to obtain more accurate and realistic material response. It must be emphasized here that crystal plasticity constitutive models incorporating strain rate sensitivity in intragranular deformations are well-established [45, 46].

Our observations in this work confirm that similar models are required for intergranular deformation studies, as well. In addition, the results found in this work can be used as guidelines in the development of grain boundary engineering (GBE) strategies in processing of material with desirable mechanical properties [47-49].

The approach introduced in this work can be applied in studies carried out in the area of GBE, particularly shedding light on the mechanical characteristics of grain boundaries in a material subjected to high strain rate loading conditions.

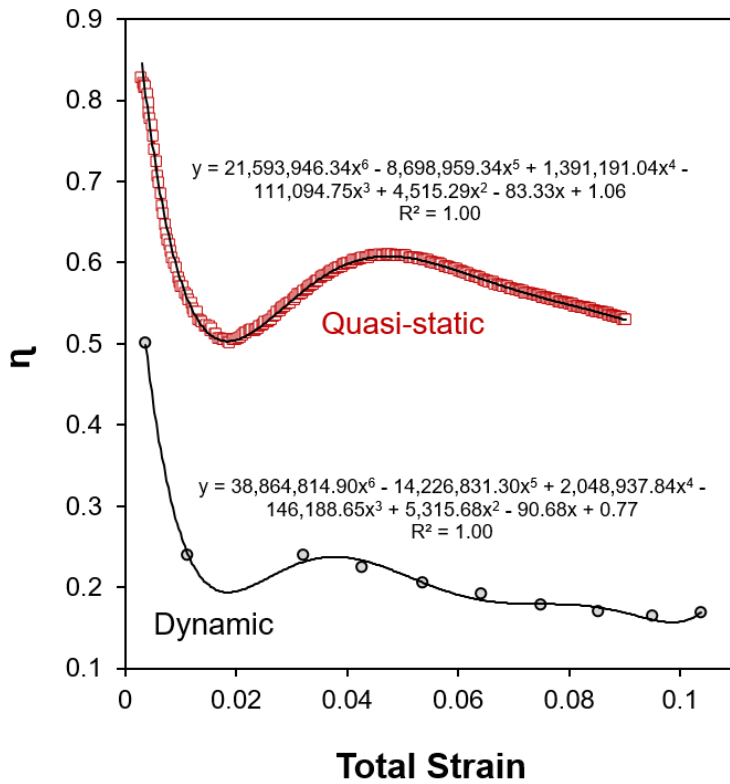


Figure 4.13. η parameter data used for direct comparing of quasi-static and dynamic results. The data shown in this figure is for a sample with grains aligned perpendicular to the loading direction.

4.5 CONCLUSIONS

Meso-scale full-field deformation characteristics of nominally pure magnesium were inspected utilizing digital image correlation under both quasi-static and dynamic loading conditions. The quasi-static mechanical response of magnesium due to differing initial grain configurations was recorded along with the evolution of intergranular cracking under uniaxial compression. The contribution of in-grain and inter-grain deformations to the total deformation of the samples was quantified. Initial grain configuration was confirmed to play a significant role in both the local and global deformation response of samples in slow deformation conditions. The relative differences in the amount of intergranular

deformation between quasi-static and dynamic cases may possibly be due to in-grain mechanisms that are more active in the dynamic regime.

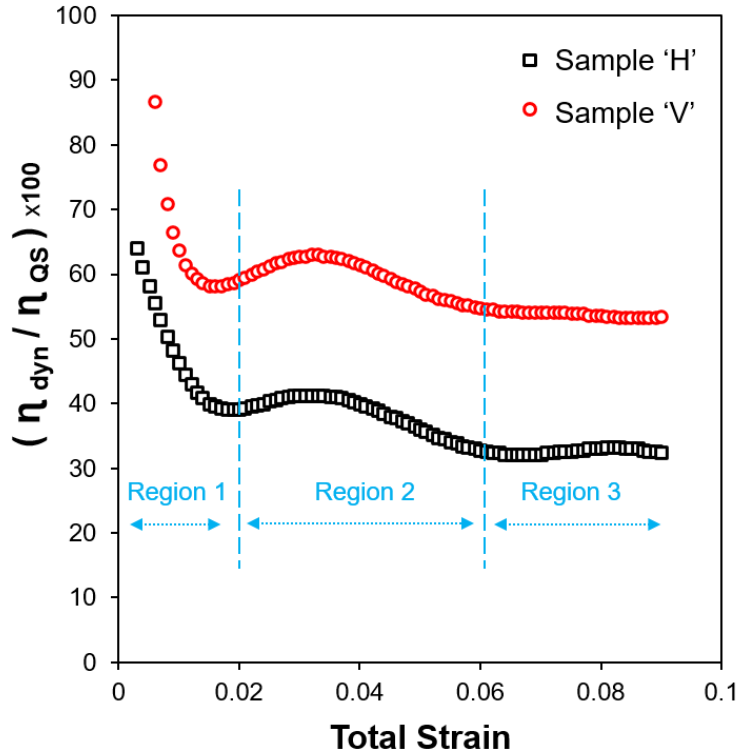


Figure 4.14. Ratio of η parameter for dynamic and quasi-static conditions versus total strain. 'Dyn' and 'QS' denote dynamic and quasi-static, respectively.

Additionally, a novel method consisting of a split Hopkinson bar apparatus and a high speed camera was used to capture local dynamic deformation of the specimen in-situ. The contributions of both inter and intragranular strain in dynamic deformation was also quantified, the former of which was found to be dependent on the grain configuration and play a substantial role in the macroscale deformation. Strain rate sensitivity levels of the material were determined and found to be related to the amount of deformation in the immediate area of grain boundaries occurring in the material. The results from this work can be used to provide a greater insight to the deformation behavior and the corresponding

mechanisms responsible in magnesium, which in turn can be applied to the modeling and crafting of systems comprised of other low ductility polycrystalline metals.

4.6 LIST OF REFERENCES

- [1] GE Dieter. Mechanical Metallurgy 3rd Ed., McGraw-Hill Book Co., New York, 1986
- [2] Hughes GM, Smith GE, Flewitt PEJ, Crocker A.G. The brittle fracture of polycrystalline zinc. Proceedings of the Royal Society. 2007. 463, 2129-2151.
- [3] Mordike BL, Ebert T. Magnesium: Properties, applications, potential. Materials Science and Engineering. 2001. 302, 37-45.
- [4] Arab SM, Akbarzadeh A. The effect of Equal Channel Angular Pressing process on the microstructure of AZ31 Mg alloy strip shaped specimen. Journal of Magnesium and Alloys. 2013. 1, 145-149.
- [5] Li B, Joshi S, Azevedo K, Ma E, Ramesh KT, Figueiredo RB, Langdon TG. Dynamic testing at high strain rates of an ultrafine-grained magnesium alloy processed by ECAP. Materials Sciences and Engineering. 2009. 517, 24-29.
- [6] Yamashita A, Horita Z, Langdon TG. Improving the mechanical properties of magnesium and a magnesium alloy through severe plastic deformation. Materials Science and Engineering. 2001. 300, 142-147.
- [7] Efstathiou C, Sehitoglu H, Lambros J. Multiscale strain measurements of plastically deforming polycrystalline titanium: Role of deformation heterogeneities. Int. J. Plast. 2010.26, 93-106.
- [8] Koohbor B, Ravindran S, Kidane A. Meso-scale strain localization and failure response of an orthotropic woven glass-fiber reinforced composite. Composites Part B-Engineering. 2015. 78, 308-318.
- [9] Raabe D, Sachtleber M, Weiland H, Scheele G, Zhao Z. Grain-scale micromechanics of polycrystal surfaces during plastic straining. Acta Materialia. 2003. 51, 1539-1560.
- [10] Tracy J, Daly S, Sevener K. Multiscale damage characterization in continuous fiber ceramic matrix composites using digital image correlation. Journal of Materials Science. 2015. 50, 5286-5299.
- [11] Zhao Z, Ramesh M, Raabe D, Cuitino AM, Radovitzky R. Investigation of three-dimensional aspects of grain-scale plastic surface deformation of an aluminum oligocrystal. Int. J. Plast. 2008. 24, 2278-2279.
- [12] Tasan CC, Hoefnagels JPM, Diehl M, Yan D, Rosters F, Raabe D. Strain localization and damage in dual phase steel investigated by coupling in-situ deformation experiments and crystal plasticity simulations. Int. J. Plast. 2014. 63, 198-210.

- [13] Di Gioacchino F, Quinta da Fonseca J. Plastic strain mapping with sub-micron resolution using digital image correlation. *Experimental Mechanics*. 2013. 53, 743-754.
- [14] Zhang Y, Topping TD, Lavernia EJ, Nutt SR. Dynamic micro-strain analysis of ultrafine-grained aluminum magnesium alloy using digital image correlation. *Metallurgical and Materials Transactions A*. 2014. 45, 47-54.
- [15] Das YB, Forsey AN, Simm TH, Perkins KM, Fitzpatrick ME, Gungor S, Moat RJ. In situ observation of strain and phase transformation in plastically deformed 301 austenitic stainless steel. *Materials and Design*. 2016. 112, 107-116.
- [16] Chen Z, Daly SH. Active slip system identification in polycrystalline metals by digital image correlation (DIC). *Experimental Mechanics*. 2017. 57, 115-127.
- [17] Di Gioacchino F, Quinta da Fonseca JQ. An experimental study of the polycrystalline plasticity of austenitic stainless steel. *Int. J. Plast.* 2015. 74, 92-109.
- [18] Guery A, Hild F, Latourte F, Roux S. Slip activities in polycrystals determined by coupling DIC measurements with crystal plasticity calculations. *Int. J. Plast.* 2016. 81, 249-266.
- [19] Bertin M, Du C, Hoefnagels JPM, Hild F. Crystal plasticity parameter identification with 3D measurements and integrated digital image correlation. *Acta Materialia*. 2016. 166, 321-331.
- [20] Guery A, Hild F, Latourte F, Roux S. Identification of crystal plasticity parameters using DIC measurements and weighted FEMU. *Mechanics of Materials*. 2016. 100, 55-71.
- [21] Bodelot L, Escobedo JP, Trujillo CP, Martinez DT, Cerreta EK, Gray T, Ravichandran G. Microstructural changes and in-situ observation of localization in OFHC copper under dynamic loading. *Int. J. Plast.* 2015. 74, 58-74.
- [22] Koohbor B, Ravindran S, Kidane, A. Effects of cell-wall instability and local failure on the response of closed-cell polymeric foams subjected to dynamic loading. *Mechanics of Materials*. 2017. (in press) DOI: 10.1016/j.mechmat.2017.03.017.
- [23] Ravindran S, Tessema A, Kidan, A. Note: Dynamic meso-scale full-field surface deformation measurement of heterogeneous materials. *Review of Scientific Instruments*. 2016. 87, 036108.
- [24] Ravindran S, Tessema A, Kidane A. Local deformation and failure mechanisms of polymer bonded energetic materials subjected to high strain rate loading. *Journal of Dynamic Behavior of Materials*. 2016. 2(1), 146-156.

- [25] Pierron F, Cheriguene R, Forquin P, Moulart R, Rossi M, Sutton MA. Performances and limitations of three ultra high speed imaging cameras for full-field deformation measurements. *Applied Mechanics and Materials*. 2011. 70, 81-86.
- [26] Koohbor B, Ravindran S, Kidane A. Experimental determination of representative volume element (RVE) size in woven composites. *Optics and Lasers in Engineering*. 2017. 90: 59-71.
- [27] Ravindran S, Koohbor B, Kidane A. Experimental characterization of meso-scale deformation mechanisms and RVE size in plastically deformed carbon steel. *Strain*. 2017. 53(1), e12217.
- [28] Chen WW, Song B. *Split Hopkinson (Kolsky) Bar: Design, Testing and Applications*. Springer. 2011.
- [29] Koohbor B, Kidane A, Lu W, Sutton MA. Investigation of the dynamic stress-strain response of compressible polymeric foam using a non-parametric analysis. *International Journal of Impact Engineering*. 2016. 91, 170-182.
- [30] Sutton MA, Orteu JJ, Schreier HW. *Image Correlation for Shape, Motion and Deformation Measurements: Basic Concepts, Theory and Applications*. 2009. Springer, NY.
- [31] Crocker AG, Flewitt PEJ, Smith GE. Computational modelling of fracture in polycrystalline materials. *International Materials Reviews*. 2005. 50, 99-124.
- [32] Wang F, Sandlobes S, Diehl M, Sharma L, Roters F, Raabe D. In-situ observation of collective grain-scale mechanics in Mg and Mg-rare earth alloys. *Acta Materialia*. 2014. 80, 77-93.
- [33] Pierron F, Zhu H, Siviour C. Beyond Hopkinson's bar. *Philosophical Transactions of the Royal Society A*. 2014. 372, 20130195.
- [34] Barnett MR, Keshavarz Z, Beer AG, Atwell D. Influence of grain size on the compressive deformation of wrought Mg-3Al-1Zn. *Acta Materialia*. 2004. 52, 5093-5103.
- [35] Dixit N, Xie KY, Hemker KJ, Ramesh KT. Microstructural evolution of pure magnesium under high strain rate loading. *Acta Materialia*. 2015. 87, 56-67.
- [36] Li B, Joshi SP, Almagri O, Ma Q, Ramesh KT, Mukai T. Rate-dependent hardening due to twinning in an ultrafine-grained magnesium alloy. *Acta Materialia*. 2012. 60, 1818-1826.
- [37] Lin XZ, Chen DL. Strain Hardening and Strain-Rate Sensitivity of an Extruded Magnesium Alloy. *Journal of Materials Engineering and Performance*. 2008. 17(6), 894-901.

- [38] Song WQ, Beggs P, Easton M. Compressive strain-rate sensitivity of magnesium–aluminum die casting alloys. *Materials and Design*. 2009. 30, 642-648.
- [39] Styczynski A, Hartig CH, Bohlen J, Letzg D. Cold rolling texture in AZ31 wrought magnesium alloy. *Scripta Materialia*. 2004. 50, 943-947.
- [40] Minarik P, Kral R, Cizek J, Chmelik F. Effect of different c/a ratio on the microstructure and mechanical properties in magnesium alloys processed by ECAP. *Acta Materialia*. 2016. 107, 83-95.
- [41] Prokoshkina D, Esin VA, Wilde G, Dvinski SV. Grain boundary width, energy and self-diffusion in nickel: Effect of material purity. *Acta Materialia*. 2013. 61, 5188-5197.
- [42] Langdon TG. Grain boundary sliding revisited: Developments in sliding over four decades. *Journal of Materials Science*. 2006. 41, 597-609.
- [43] Langdon T. Grain boundary sliding as a deformation mechanism during creep. *Philosophical Magazine*. 1970. 22, 689-700.
- [44] Lenoir N, Bornert M, Desrues J, Besuelle P, Viggiani G. Volumetric digital image correlation applied to X-ray microtomography images from triaxial compression tests on Argillaceous rock. *Strain*. 2007. 43(3), 193-205.
- [45] Barlat F, Glazov MV, Brem, JC, Lege DJ. A simple model for dislocation behavior, strain and strain rate hardening evolution in deforming aluminum alloys. *Int. J. Plast.* 2002. 18, 919-939.
- [46] Salem AA, Kalidindi SR, Semiatin SL. Strain hardening due to deformation twinning in α -titanium: Constitutive relations and crystal-plasticity model. *Acta Materialia*. 2005. 53, 3495-3502.
- [47] Cao W, Xia S, Bai Q, Zhang W, Zhou B, Li Z, Jiang L. Effects of initial microstructure on the grain boundary network during grain boundary engineering in Hastelloy N alloy. *Journal of Alloys and Compounds*. 2017. 704, 724-733.
- [48] Randle V. Twinning-related grain boundary engineering. *Acta Materialia*. 2004. 52, 4067-4081.
- [49] Wantanabe T, Tsurekawa S. Toughening of brittle materials by grain boundary engineering. *Materials Science and Engineering A*. 2004. 387-389, 447-455.

CHAPTER 5

RELATIVE GRAIN SIZE COMPARISON STUDY

5.1 ABSTRACT

In the interest of a more complete investigation into the local microstructural response of pure magnesium, we present a brief experimental work examining the grain scale strain of several quasi-static tests under tension. The specimens used here feature substantially smaller grain sizes than those examined in the previous chapters. The main objective in this work was to verify potential effects of material grain size on the localized strain activity, while simultaneously testing the effectiveness of DIC techniques at considerably small grain sizes with sufficient spatial resolution.

Our results demonstrated that DIC analysis reveals that many aspects of the grain boundary region deformation observed in this work were similar to those seen in Chapters 3 and 4. In addition, more general comparisons between the compression and tensile tests are discussed.

Results unique to this work include evidence that relative grain size differences within a given sample affect the amount, degree and location of the concentrated deformation activity. Also, the current study confirms previous hypotheses regarding the whereabouts of structurally weak points within a multi-scale grain network. Once again, this strain localization is likely a working combination of formerly discussed deformation mechanisms forming in the microstructure.

5.2 SAMPLE PREPARATION

Nominally pure (99.9%) H24 temper rolled magnesium was used in the present work. Samples were cut from a magnesium sheet using a waterjet cutter and were annealed in an oven at 550 C for 6 hours to induce grain growth. This rolled magnesium exhibited grain sizes of approximately 10 μm before heat treatment and 50 μm after annealing. The latter was selected for analysis in order to better study the grain boundary region activity under high magnification. It should be noted that the samples grain size heterogeneity possibly resulted from exposure to non-uniform ambient temperatures.

Subsequently, the surfaces of the samples were polished using incremental grits of sandpaper and a range of aqueous alumina powders. Each specimen was then etched for 2 minutes in a solution consisting of the same ingredients mentioned in previous chapters. After etching, a surface area of interest on each sample was specified and marked using a hardness tester in a manner similar to a different work studying microstructure at high magnification [1]. Indentation patterns were placed on a part of the surface free of defects and imaged prior to applying the speckle configuration.

Because of the high level of magnification required for these experiments, a much more refined speckle pattern was needed in the present work to detail the grain boundary region displacements. To do this, and facilitate accurate DIC measurements, the speckle pattern was applied to the polished surfaces by roughening the area of interest with an ultra-fine grained powder (1000 grit).

This surface roughening created fine marks and divots which helped generate sufficient contrast to be recognized by the DIC software. This speckling technique is slightly less rigorous and is not commonly implemented.

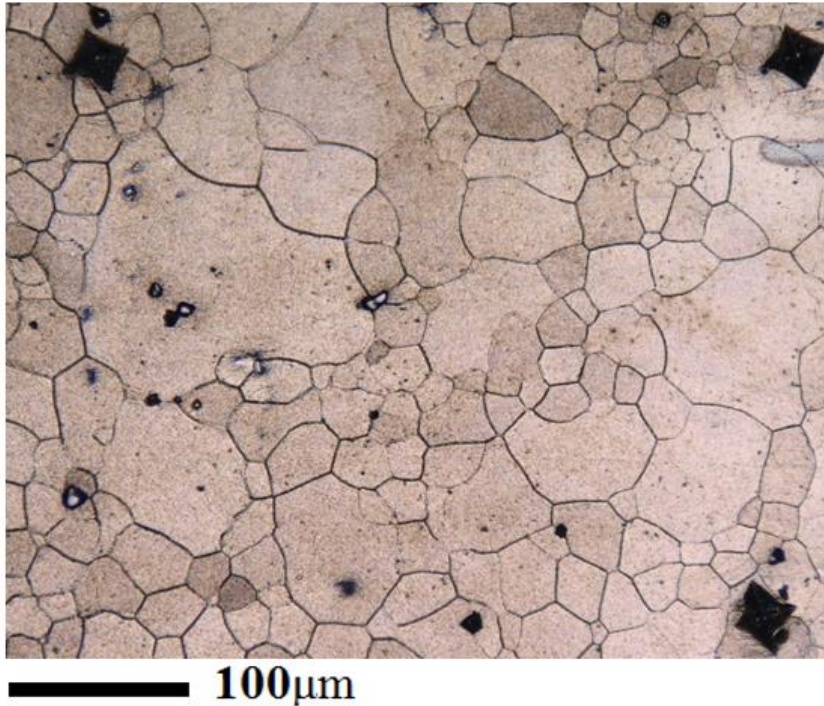


Figure 5.1. Indentation pattern in three corners to map an area of interest.

5.3 EXPERIMENTAL SETUP

Images of the events were recorded with 5 MP CCD camera (Grasshopper GS3-U3-51S5M-C, FLIR) fixed to a microscope lens at 11.5x magnification. The frame rate used was 1 image every 4 seconds. The sample area of interest was captured in a field of view of approximately $440 \times 368 \mu\text{m}^2$ at a spatial resolution of approximately $0.18 \mu\text{m}/\text{pixel}$. The tensile load was applied at a speed of $5 \mu\text{m}$ per second which corresponded to a sample strain rate of approximately $2.5 \times 10^{-4}/\text{s}$. The motor of the tensile machine was synchronized with the lateral governor of the vertically held camera such that the area of interest was controlled to remain within the field of view during deformation.

Post-processing was done in VIC-2D software and images of each sample were correlated using subset and step sizes of 67 and 2 pixels respectively, with a filter size of 15. These parameters were carefully selected in order to produce the highest resolution

images to best capture the grain boundary activity, and were based on DIC specifications [2]. Full-field strain maps featuring all three strain components (ϵ_{xx} , ϵ_{yy} , ϵ_{xy}) of each sample were developed and the microstructural grain maps were overlaid on each plot to provide context regarding the whereabouts of the heterogeneous strain patterns.

For both of the tensile specimens in this work, each showed similar grain arrangements to each other prior to testing and were loaded until a sufficient degree of global strain was achieved.

5.4 RESULTS AND DISCUSSION

In-situ DIC analysis revealed that both samples exhibited comparable localized deformation features to one another. The surface strain contour plots are shown in Figures 5.2 and 5.3. In addition, we can compare the results here with previous analysis of our cast magnesium samples tested in compression as shown in Figure 5.4. For each sample tested in Figures 5.2 and 5.3, the majority of the grains were approximately 50 μm in size. However the individual grains themselves had sizes in the range of about 20 μm to 100 μm .

This wide range of grain sizes within each sample is fundamentally different than our previous specimens tested quasi-statically (see Figures 4.7 and 5.4) in that, here, the relative difference in grain size within each sample was as much as ten times in some areas. By comparison, our compression experiments yielded grains that were generally the same size as each other with minor variations.

Similar to the work in chapter 4, the full field strain maps in all the figures shown here display by rows each of the three major strain components. Beginning with the axial strain ϵ_{xx} at the top, followed by ϵ_{yy} and ϵ_{xy} .

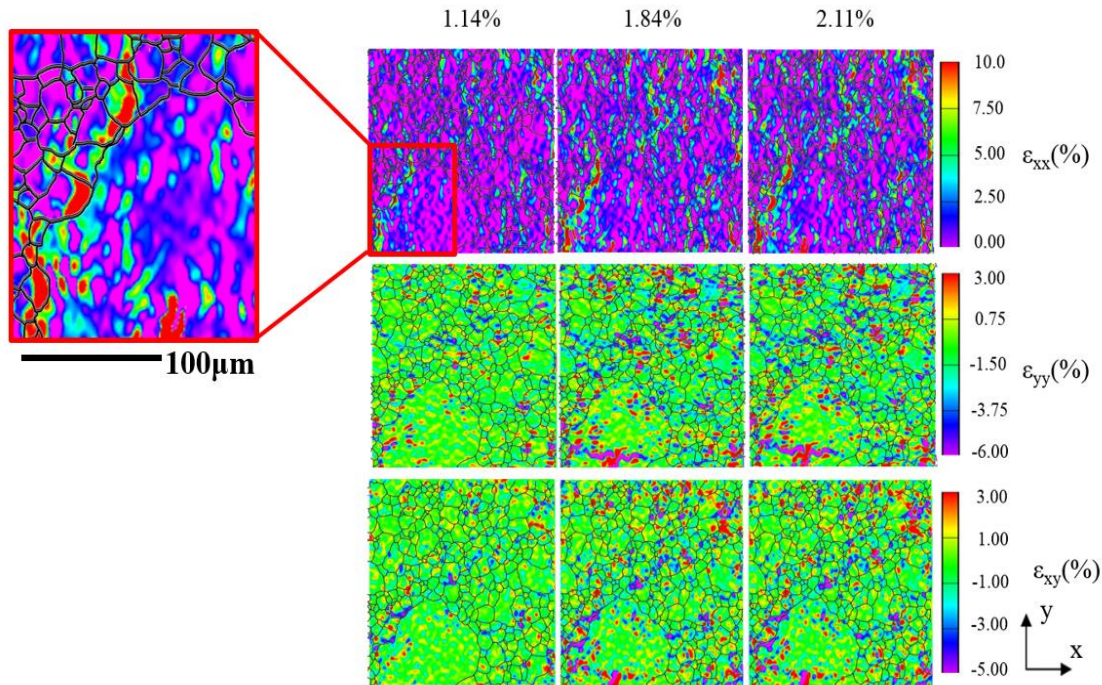


Figure 5.2. Full-field contour strain map of sample 1 featuring all three strain components shown by row. Columns represent the degree of global strain.

The plot range of values for the scale of each contour was carefully chosen to best display the more prominent regions of concentrated strain as they relate to the overall microstructure. As mentioned previously, the global strain was calculated with DIC-based ‘virtual extensometer’ feature, which gives accurate measurements with sub-pixel resolution. Which has been shown to be more precise than calculating from traditional fixture displacements.

In this set of experiments, the areas receiving the highest amount of localized strain for each component again appeared at grain boundary regions and junction points, while the degree of in-grain deformation is again observed to be comparatively small. This is most apparent when examining the ϵ_{xx} and ϵ_{xy} maps, where, in the more concentrated regions ϵ_{xx} sees values as high as 14% despite the global strain being less than 2%. However, unlike the previous experiments, there is not as much evidence of grain

boundary activity when analyzing the transverse strain, which may be due to the fact that Poisson's effect is not as pronounced in this rolled magnesium which was annealed and these maps focus on intervals at relatively lower amounts of global strain.

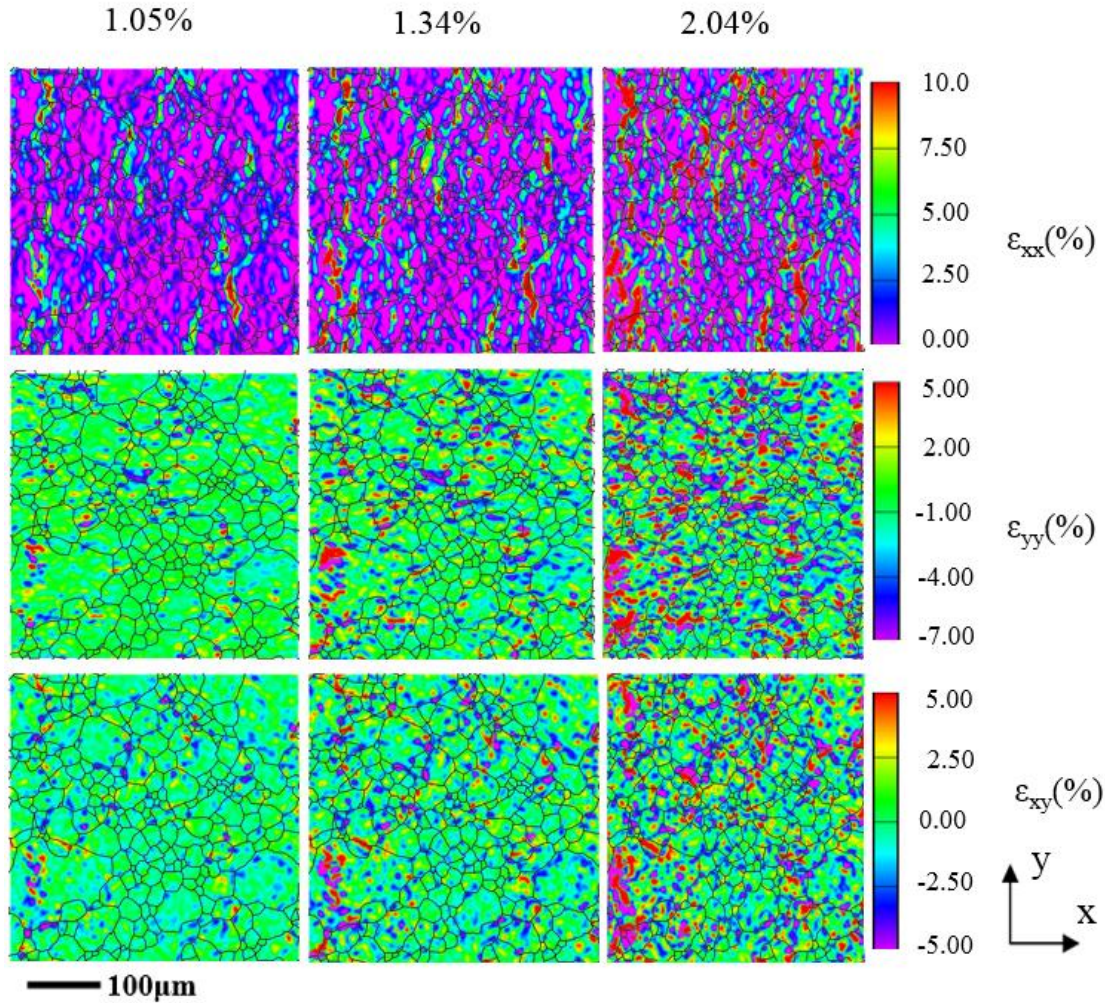


Figure 5.3. Sample 2 contour plots.

Furthermore, it is seen that in both of the experiments in the current work that the highest concentrations of the strain occur preferentially around the relatively larger grains, and it appears to be distributed in a more unpredictable manner in the areas around the smaller grains. This suggests that the difference in the relative grain size within a single sample influences the sites of the localization. This notion is supported when examining

the large grained samples with a more consistent grain size distribution tested (Figures 4.7 and 5.4) where the strain concentrations occur at the grain boundaries but in a less predictable manner than in our smaller grained samples.

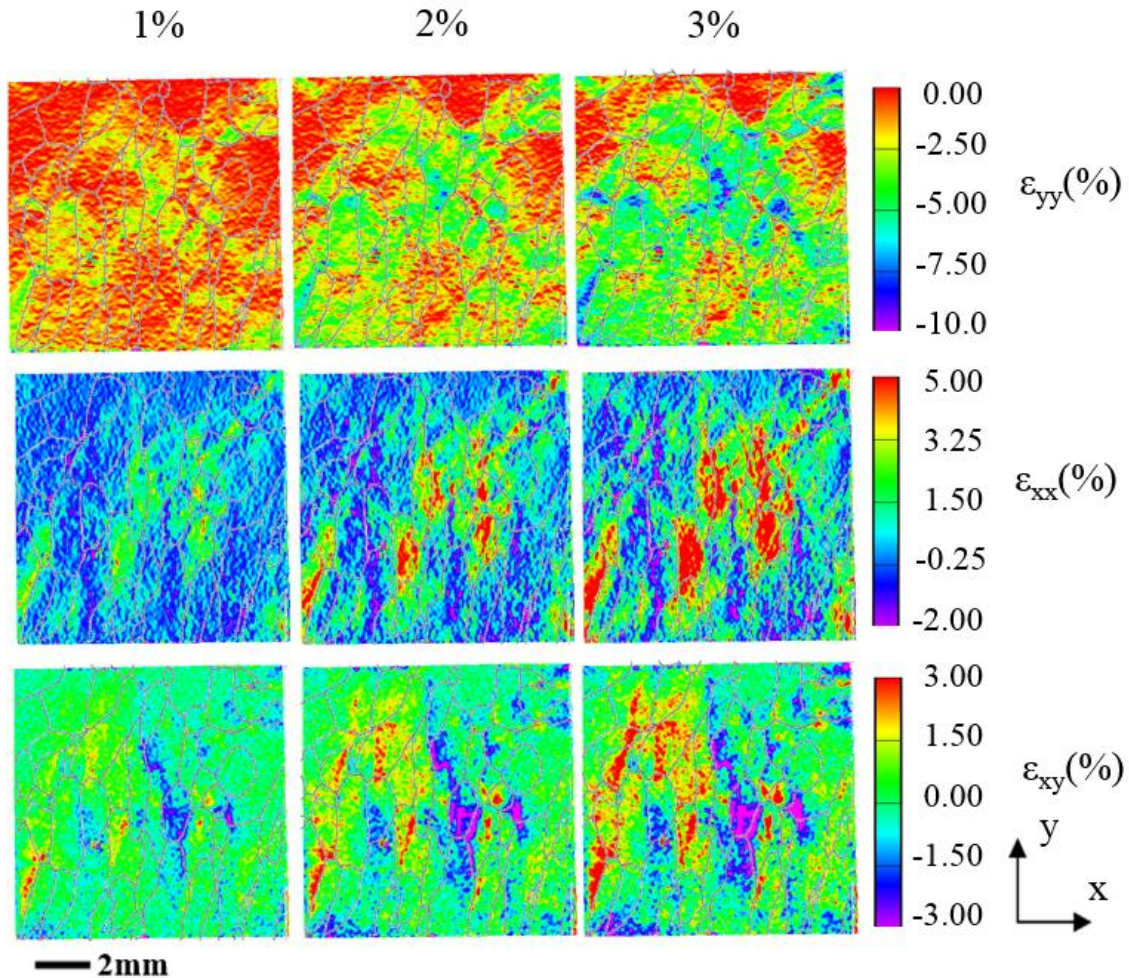


Figure 5.4. Contour strain maps of large grained magnesium sample tested under compression. This sample, in addition to the one featured in Figure 4.7 display a relatively homogenous grain size distribution.

The amount and degree of the localization is also less by comparison. The effects of a multi-scale microstructure in metals on the global response have been documented in the literature; a pair of studies done on Al-Zr alloys suggests that incorporating larger sized grains into a nanocrystalline microstructural matrix serves to make them more unstable in regions where larger grains are directly adjacent to small grains [3, 4]. While the local

response may be compromised, a related work done by Witkin, et al [5] on a Mg-Al alloy engineered to have a heterogeneous grain size distribution revealed that the overall strength and ductility of the alloy increased after modification. However, it was reiterated that specimen yielding presumably initiated and progressed in the regions around larger grains.

The concentrated deformation occurring within the larger grains may be signs of twinning nucleation, which is more probable inside larger sized grains. This has been shown in Mg alloys even at low levels of global strain [6, 7]. In addition, the concentrated in-grain strain may be evidence of slip occurring in the microstructure, since this is known to happen in magnesium alloys under tension; irrespective of the rolling or transverse directions [8, 9]. Most likely, however, is the high possibility of large compatibility stresses occurring as a direct result of the grain size difference.

In summary, it is shown here that sufficient spatial resolution is attained for these tests; thereby demonstrating the effectiveness of DIC analysis at considerably small length scales. The in-situ localized strain response of rolled pure magnesium was characterized and it was observed that the boundary regions in proximity to relatively larger grains appear to be more susceptible to damage and failure initiation than areas of the microstructure consisting of comparable grain sizes. In light of these observations, we hypothesize that this phenomenon may occur regardless of the average grain size.

5.5 LIST OF REFERENCES

- [1] Ravindran S, Koohbor B, Kidane A. Experimental characterization of meso-scale deformation mechanisms and the RVE size in plastically deformed carbon steel. *Strain*. 2016; e122, doi: 10.1111/str.12217.
- [2] Sutton MA, Orteu JJ, Schreier HW. *Image Correlation for Shape, Motion and Deformation Measurements*. Springer, New York. 2009.
- [3] Rittner MN, Weertman JR, Eastman JA, Yoder KB, Stone DS. Mechanical behavior of nanocrystalline Aluminum-Zirconium. *Material Science and Engineering*. 1997. 237A, 185.
- [4] Gertman VY, Birringer R. On the room-temperature grain growth in nanocrystalline copper. *Scripta Metallurgica et Materialia*. 1994. 30, 577-581.
- [5] Witkin D, Lee Z, Rodriguez R, Nutt S, Lavernia E. Al-Mg alloy with bimodal grain size for high strength and increased ductility. *Scripta Materialia*. 2003. 49, 297-302.
- [6] Dobron P, Frantisek C, Sangbong Y, et al. Grain size effects on deformation twinning in an extruded mg alloy in compression. *Scripta Materialia*. 2011. 65, 424-427.
- [7] del Valle JA, Carreno F, Ruano OA. Influence of texture and grain size on work hardening and ductility in magnesium-based alloys processed by ECAP and rolling. *Acta Materialia*. 2006. 54, 4247-4259.
- [8] Agnew SR, Duygulu O. Plastic anisotropy and the role of non-basal slip in magnesium alloy AZ31B. *International Journal of Plasticity*. 2005. 21, 1161-1193.
- [9] Keshavarz Z, Barnett MR. EBSD analysis of deformation modes in Mg-3Al-1Zn. *Scripta Materialia*. 2006. 55, 915-918.

CHAPTER 6

SUMMARY AND RECOMMENDATIONS

6.1 SUMMARY

The experimental works presented in this manuscript document the meso-scale microstructural deformation activity of pure magnesium under various loading conditions; while simultaneously demonstrating the practicality of DIC analysis in this regard. This method allowed for in-depth study of both quasi-static and dynamic events by providing high resolution in-situ data for mapping the full-field strain behavior of several variants of pure magnesium. From this, we were able to discuss several hypotheses regarding the nature of the grain boundary action and global response; specifically making the following set of conclusions:

- For all magnesium specimens tested, it was verified based on the quantitative full-field strain measurements that the grain boundaries are mechanically weak and fracture initiation takes place in these regions. Also, it was hypothesized that the calculated in-grain deformation activity seen in all samples tested, was a working combination of several deformation mechanisms known to be active in magnesium.
- In general, the overall contribution of grain boundary region strain to the global response is significant throughout the deformation process and can vary at low levels of global strain depending on the initial grain configurations.
- The global constitutive response of the cast magnesium at low levels of strain is also suspected to be dependent on the grain arrangement.

- Grain boundary region deformation captured in the dynamic regime was seen to be more prominently featured at the triple junction points.
- It is hypothesized that large relative differences in grain size within a single specimen may influence the locations of mechanically susceptible failure regions in the microstructure, as well as the possible formation various deformation modes, most likely as a result of large compatibility stresses arising in these regions.
- Finally, it can be concluded that DIC offers a means to effectively quantify the local response of a polycrystalline metal subjected to a wide range of applied strain rates at multiple length scales at sufficiently high spatial resolution to identify localized activity in the immediate vicinity of grain boundary regions.

6.2 RECOMMENDATIONS

Based on the observations made here from the experimental studies described in this work, some recommendations regarding future work include attempting to further characterize the full-field material strain activity as it directly relates to the known deformation mechanisms of magnesium. As stated previously, DIC by itself cannot confirm the presence of specific modes of mechanical behavior occurring in the material. Instead, DIC provides a working contour map regarding the whereabouts of concentrated regions of surface strain taking place. In previous works concerning the study of specific deformation mechanisms in metals, Electron Backscatter Diffraction (EBSD) was typically used to map the texture and confirm the presence of these phenomenon. This technique is one of the most cited methods of which to definitively identify the regions featuring twinning activity. However, a limitation of EBSD is that it is unable to compute strain

occurring at the surface, instead it provides texture evolution data in the absence of quantitative material deformation information.

One could potentially utilize EBSD in conjunction with a DIC-based method to specifically map the grain scale activity both in quasi-static and dynamic regimes. In addition to a more complete study of the deformation mechanisms, a further look into the texture evolution in cast versus rolled magnesium could offer a better idea of how the material surface changes with respect to preparation process. This approach could be paired with a DIC-based study on the heterogeneous strain patterns.

Also, a more comprehensive look into the fundamental differences between pure magnesium and magnesium alloys could be achieved by adopting the methodologies described in this manuscript. One could compare the granular activity of both materials and make conclusions based on the presumed variations in the localized deformation behavior.

Most importantly, the versatility of the methods described in this work can potentially extend to effectively characterizing the microstructural response of virtually any polycrystalline system at high resolution subjected to a wide range of applied strain rates.

BIBLIOGRAPHY

- Agnew SR, Duygulu O. Plastic anisotropy and the role of non-basal slip in magnesium alloy AZ31B. *International Journal of Plasticity*. 2005. 21, 1161-1193.
- Arab SM, Akbarzadeh A. Effect of equal channel angular pressing process on the microstructure of AZ31 Mg alloy strip shaped specimens. *Journal of Magnesium and Alloys*. 2013. 1, 145-149.
- Balogh L, Niezgoda SR, Kanjarla AK, Brown DW, Clausen B, Liu W, Tome CN. Spatially resolved in situ strain measurements from an interior twinned grain in bulk polycrystalline AZ31 alloy. *Acta Materialia*. 2013. 61, 3612-3620.
- Barlat F, Glazov MV, Brem, JC, Lege DJ. A simple model for dislocation behavior, strain and strain rate hardening evolution in deforming aluminum alloys. *Int. J. Plast.* 2002. 18, 919-939.
- Barnett MR, Keshavarz Z, Beer AG, Atwell D. Influence of grain size on the compressive deformation of wrought Mg-3Al-1Zn. *Acta Materialia*. 2004. 52, 5093-5103.
- Bertin M, Du C, Hoefnagels JPM, Hild F. Crystal plasticity parameter identification with 3D measurements and integrated digital image correlation. *Acta Materialia*. 2016. 166, 321-331.
- Bieler TR, et al. The role of heterogeneous deformation on damage nucleation at grain boundaries in single phase metals. *Int. J. Plast.* 2009. 25, 1655-1683
- Bodelot L, Escobedo JP, Trujillo CP, Martinez DT, Cerreta EK, Gray T, Ravichandran G. Microstructural changes and in-situ observation of localization in OFHC copper under dynamic loading. *Int. J. Plast.* 2015. 74, 58-74.
- Cao W, Xia S, Bai Q, Zhang W, Zhou B, Li Z, Jiang L. Effects of initial microstructure on the grain boundary network during grain boundary engineering in Hastelloy N alloy. *Journal of Alloys and Compounds*. 2017. 704, 724-733.
- Chen Z, Daly SH. Active slip system identification in polycrystalline metals by digital image correlation (DIC). *Experimental Mechanics*. 2017. 57, 115-127.
- Chen WW, Song B. *Split Hopkinson (Kolsky) Bar: Design, Testing and Applications*. Springer. 2011.

Chichilia DR, Ramesha KT, Hemkera KJ. The high-strain rate response of alpha-titanium: experiments, deformation mechanisms and modeling. *Acta Materialia*. 1998. 46, 1025-1043.

Chino Y, Kimura K, Hakamada M, Mabuchi M. Mechanical anisotropy due to twinning in an extruded AZ31 Mg alloy. *Materials Science and Engineering A*. 2008. 485, 311-317.

Chu TC, Ranson WF, Sutton MA. Applications of digital-image-correlation techniques to experimental mechanics. *Experimental Mechanics*. 1985. 25, 232-244.

Crocker AG, Flewitt PEJ, Smith GE. Computational modelling of fracture in polycrystalline materials. *International Materials Reviews*. 2005. 50, 99-124.

Das YB, Forsey AN, Simm TH, Perkins KM, Fitzpatrick ME, Gungor S, Moat RJ. In situ observation of strain and phase transformation in plastically deformed 301 austenitic stainless steel. *Materials and Design*. 2016. 112, 107-116.

Dobron P, Chmelik F, Yi S, Parfenenko K, Letzig D, Bohlen J. Grain size effects on the deformation twinning in an extruded magnesium alloy tested in compression. *Scripta Materialia*. 2011. 65, 424-427.

Dieter GE. *Mechanical Metallurgy* 3rd Ed. McGraw-Hill Book Co., New York, 1986.

Di Gioacchino F, Quinta da Fonseca JQ. An experimental study of the polycrystalline plasticity of austenitic stainless steel. *Int. J. Plast.* 2015. 74, 92-109.

Di Gioacchino F, Quinta da Fonseca J. Plastic strain mapping with sub-micron resolution using digital image correlation. *Experimental Mechanics*. 2013. 53, 743-754.

Dixit N, Hazeli K, Ramesh KT. Twinning in magnesium under dynamic loading. *EPJ Web of Conferences*. 2015. 15, doi: 10.1051/epjconf/20159402018.

Dixit N, Xie KY, Hemker KJ, Ramesh KT. Microstructural evolution of pure magnesium under high strain rate loading. *Acta Materialia*. 2015. 87, 56-67.

Dudamell NV, Ulacia I, Galvez F, Yi S, Bohlen J, Letzig D, Hurtado I, Perez-Prado MT. Twinning and grain subdivision during dynamic deformation of a Mg AZ31 sheet alloy at room temperature. *Acta Materialia*. 2011. 59, 6949-6962.

Efstathiou C, Sehitoglu H, Lambros J. Multiscale strain measurements of plastically deforming polycrystalline titanium: Role of deformation heterogeneities. *Int. J. Plast.* 2010.26, 93-106.

Galiyev A, Kaibyshev R, Gottstein G. Correlation of plastic deformation and dynamic recrystallization in magnesium alloy ZK60. *Acta Materialia*. 2001. 49, 1199-1207.

- Gertman VY, Birringer R. On the room-temperature grain growth in nanocrystalline copper. *Scripta Metallurgica et Materialia*. 1994. 30, 577-581.
- Guery A, Hild F, Latourte F, Roux S. Slip activities in polycrystals determined by coupling DIC measurements with crystal plasticity calculations. *Int. J. Plast.* 2016. 81, 249-266.
- Guery A, Hild F, Latourte F, Roux S. Identification of crystal plasticity parameters using DIC measurements and weighted FEMU. *Mechanics of Materials*. 2016. 100, 55-71.
- Gutkin MY, Ovid'ko IA, Skiba NV. Crossover from grain boundary sliding to rotational deformation in nanocrystalline materials. *Acta Materialia*. 2003. 51, 4059-4071.
- Hazeli K, Kingstedt OT, Kannan V, Ravichandran G, Ramesh KT. Strain evolution and twinning modes in magnesium single crystal. Preprint submitted to Elsevier. 2016.
- Hong X, Godfrey A, Liu W, Orozco-Caballero A, Quinta da Fonseca J. Effect of pre-existing twinning on strain localization during deformation of a magnesium alloy. *Materials Letters*. 2017. doi: <http://d.doi.org/10.1016/j.matlet.2017.07.077>.
- Hughes GM, Smith GE, Flewitt PEJ, Crocker A.G. The brittle fracture of polycrystalline zinc. *Proceedings of the Royal Society*. 2007. 463, 2129-2151.
- Humphreys FJ. Characterisation of fine-scale microstructures by electron backscatter diffraction (EBSD). *Scripta Materialia*. 2004. 51, 771-776.
- Hussein RO, Northwood DO. Improving the performance of magnesium alloys for automotive applications, *High Performance and Optimum Design of Structures and Materials*. 2014. 137, 1743-3509.
- Hutchinson JW, Neale KW. Influence of strain-rate sensitivity on necking under uniaxial tension. *Acta Metallurgica*. 1977. 25, 839-846.
- Ishikawa K, Watanabe H, Mukai T. High strain rate deformation behavior of an AZ91 magnesium alloy at elevated temperatures. *Materials Letters*. 2005. 59, 1511-1515.
- Kappos AJ. *Dynamic loading design of structures*. Spon Press. New York, 2002.
- Ke M, Hackney SA, Milligan WW, Aifantis EC. Observation and measurement of grain rotation and plastic strain in nanostructured metal thin films. *Nanostructured Materials*. 1995. 5, 689-697.
- Keshavarz Z, Barnett MR. EBSD analysis of deformation modes in Mg-3Al-1Zn. *Scripta Materialia*. 2006. 55, 915-918.

Koike J. Enhanced deformation mechanisms by anisotropic plasticity in polycrystalline Mg alloys at room temperature. *Metallurgical and Materials Transactions: Physical Metallurgy and Materials Science*, A. 2005. 36, 1689-1696.

Koike J, Ohyama R, Kobayashi T, Suzuki M, Maruyama K. Grain-boundary sliding in AZ31 magnesium alloys at room temperature to 523 K. *Materials Transactions*. 2003. 44, 445-451.

Koohbor B, Ravindran S, Kidane, A. Effects of cell-wall instability and local failure on the response of closed-cell polymeric foams subjected to dynamic loading. *Mechanics of Materials*. 2017. (in press) DOI: 10.1016/j.mechmat.2017.03.017.

Koohbor B, Ravindran S, Kidane A. Experimental determination of representative volume element (RVE) size in woven composites. *Optics and Lasers in Engineering*. 2017. 90: 59-71.

Koohbor B, Kidane A, Lu W, Sutton MA. Investigation of the dynamic stress-strain response of compressible polymeric foam using a non-parametric analysis. *International Journal of Impact Engineering*. 2016. 91, 170-182.

Koohbor B, Kidane A, Lu W, Sutton MA. Investigation of the dynamic stress-strain response of compressible polymeric foam using a non-parametric analysis. *International Journal of Impact Engineering*. 2016. 91, 170-182.

Koohbor B, Ravindran S, Kidane A. Meso-scale strain localization and failure response of an orthotropic woven glass-fiber reinforced composite. *Composites Part B-Engineering*. 2015. 78, 308-318.

Langdon T. Grain boundary sliding as a deformation mechanism during creep. *Philosophical Magazine*. 1970. 22, 689-700.

Langdon TG. Grain boundary sliding revisited: Developments in sliding over four decades. *Journal of Materials Science*. 2006. 41, 597-609.

Lenoir N, Bornert M, Desrues J, Besuelle P, Viggiani G. Volumetric digital image correlation applied to X-ray microtomography images from triaxial compression tests on Argillaceous rock. *Strain*. 2007. 43(3), 193-205.

Li B, Joshi S, Azevedo K, Ma E, Ramesh KT, Figueiredo RB, Langdon TG. Dynamic testing at high strain rates of an ultrafine-grained magnesium alloy processed by ECAP. *Materials Science and Engineering A*. 2009. 517, 24-29.

Li B, Joshi SP, Almagri O, Ma Q, Ramesh KT, Mukai T. Rate-dependent hardening due to twinning in an ultrafine-grained magnesium alloy. *Acta Materialia*. 2012. 60, 1818-1826.

- Liu Q, Jensen J, Hansen N. Effect of grain orientation on deformation structure in cold-rolled polycrystalline aluminum. *Acta Materialia*. 1998. 46, 5819-5838.
- Lin XZ, Chen DL. Strain Hardening and Strain-Rate Sensitivity of an Extruded Magnesium Alloy. *Journal of Materials Engineering and Performance*. 2008. 17(6), 894-901.
- Malvern LE. Plastic wave propagation in a bar of material exhibiting a strain rate effect. *Quarterly of Applied Mathematics*. 1951. 8, 405-411.
- Meyers M. *Dynamic behavior of materials* 1st ed. Wiley-interscience, New York, 1994. 1-4.
- Meyers MA, Vohringer O, Lubarda VA. The onset of twinning in metals: a constitutive description. *Acta mater*. 2001. 49, 4025-4039.
- Minarik P, Kral R, Cizek J, Chmelik F. Effect of different c/a ratio on the microstructure and mechanical properties in magnesium alloys processed by ECAP. *Acta Materialia*. 2016. 107, 83-95.
- Molodov KD, Al-Samman T, Molodov DA. On the diversity of the plastic response of magnesium in plane strain compression. *Materials Science and Engineering A*. 2016. 651, 63-68.
- Mordike BL, Ebert T, Magnesium: Properties, applications, potential. *Materials Science and Engineering A*. 302 (2001) 37-45.
- Mukai T, Yamanoi M, Watanabe H, Ishikawa K, Higashi K. Effect of grain refinement on tensile ductility in ZK60 magnesium alloy under dynamic loading. *Materials Transactions*. 2001. 42, 1177-1181.
- Panicker R, Chokshi AH, Mishra RK, Verma R, Krajewski PE. Microstructural evolution and grain boundary sliding in a superplastic magnesium AZ31 alloy. *Acta Materialia*. 2009. 57, 3683-3693.
- Pierron F, Cheriguen R, Forquin P, Moulart R, Rossi M, Sutton MA. Performances and limitations of three ultra high speed imaging cameras for full-field deformation measurements. *Applied Mechanics and Materials*. 2011. 70, 81-86.
- Pierron F, Zhu H, Siviour C. Beyond Hopkinson's bar. *Philosophical Transactions of the Royal Society A*. 2014. 372, 20130195.
- Prokoshkina D, Esin VA, Wilde G, Dvinski SV. Grain boundary width, energy and self-diffusion in nickel: Effect of material purity. *Acta Materialia*. 2013. 61, 5188-5197.
- Raabe D, Sachtleber M, Weiland H, Scheele G, Zhao Z. Grain-scale micromechanics of polycrystal surfaces during plastic straining. *Acta Materialia*. 2003. 51, 1539-1560.

Randle V. Twinning-related grain boundary engineering. *Acta Materialia*. 2004. 52, 4067-4081.

Ravindran S, Tessema A, Kidane A. Multiscale damage evolution in polymer bonded sugar under dynamic loading. *Mechanics of Materials*. 2017. 114, 97-106.

Ravindran S, Koohbor B, Kidane A. Experimental characterization of meso-scale deformation mechanisms and the RVE size in plastically deformed carbon steel. *Strain*. 2016; e122, doi: 10.1111/str.12217.

Ravindran S, Tessema A, Kidan, A. Note: Dynamic meso-scale full-field surface deformation measurement of heterogeneous materials. *Review of Scientific Instruments*. 2016. 87, 036108.

Ravindran S, Tessema A, Kidane A. Local deformation and failure mechanisms of polymer bonded energetic materials subjected to high strain rate loading. *Journal of Dynamic Behavior of Materials*. 2016. 2(1), 146-156.

Rittner MN, Weertman JR, Eastman JA, Yoder KB, Stone DS. Mechanical behavior of nanocrystalline Aluminum-Zirconium. *Material Science and Engineering*. 1997. 237A, 185.

Salem AA, Kalidindi SR, Semiatin SL. Strain hardening due to deformation twinning in α -titanium: Constitutive relations and crystal-plasticity model. *Acta Materialia*. 2005. 53, 3495-3502.

Schwaiger R, Moser B, Dao M, Chollacoop N, Suresh S. Some critical experiments on the strain-rate sensitivity of nanocrystalline nickel. *Acta Materialia*. 2003. 51, 5159-5172.

Shaw BA. Corrosion Resistance of Magnesium Alloys, *ASM Handbook*. 2003. 13A, 692-696.

Shimokawa T, Nakatani A, Kitagawa H. Grain size dependence of the relationship between intergranular and intragranular deformation of nanocrystalline Al by molecular dynamics simulations. *Physical Review B*. 2005. 71, 224110.

Somekawa H, Mukai T. Effect of grain refinement on fracture toughness in extruded pure magnesium. *Scripta Materialia*. 2005. 53, 1059-1064.

Song WQ, Beggs P, Easton M. Compressive strain-rate sensitivity of magnesium-aluminum die casting alloys. *Materials and Design*. 2009. 30, 642-648.

Steinberg DJ, Cochran SG, Guinan MW. A constitutive model for metals applicable at high strain rate. *Journal of Applied Physics*. 1980. 51, 1498.

Styczynski A, Hartig C, Bohlen J, Letzg D. Cold rolling texture in AZ31 wrought magnesium alloy. *Scripta Materialia*. 2004. 50, 943-947.

Sutton MA, Orteu JJ, Schreier HW. *Image Correlation for Shape, Motion and Deformation Measurements: Basic Concepts, Theory and Applications*. 2009. Springer, NY.

Sutton MA, Wolters WJ, Peters WH, Ranson WF, McNeill SR. Determination of displacements using an improved digital image correlation method. *Image and Vision Computing*. 1983. 1, 133-139.

Tasan CC, Hoefnagels JPM, Diehl M, Yan D, Rosters F, Raabe D. Strain localization and damage in dual phase steel investigated by coupling in-situ deformation experiments and crystal plasticity simulations. *Int. J. Plast.* 2014. 63, 198-210.

Tracy J, Daly S, Sevener K. Multiscale damage characterization in continuous fiber ceramic matrix composites using digital image correlation. *Journal of Materials Science*. 2015. 50, 5286-5299.

Tucker MT, Horstemeyer MF, Gullett PM, El Kadiri H, Whittington WR. Anisotropic effects on the strain rate dependence of a wrought magnesium alloy. *Scripta Materialia*. 2009. 60, 182-185.

del Valle JA, Carreno F, Ruano OA. Influence of texture and grain size on work hardening and ductility in magnesium-based alloys processed by ECAP and rolling. *Acta Materialia*. 2006. 54, 4247-4259.

Van Swygenhoven H, Derlet PM. Grain boundary sliding in nanocrystalline fcc metals. *Physical Review B*. 2001. 64, 224105.

Wang F, Sandlobes S, Diehl M, Sharma L, Roters F, Raabe D. In-situ observation of collective grain-scale mechanics in Mg and Mg-rare earth alloys. *Acta Materialia*. 2014. 80, 77-93.

Wang YM, Ma E. Strain hardening, strain rate sensitivity, and ductility of nanostructured metals. *Materials Science and Engineering A*. 2004. 375-377, 46-52.

Watanabe T, Tsunekawa S. Toughening of brittle materials by grain boundary engineering. *Materials Science and Engineering A*. 2004. 387-389, 447-455.

Watanabe H, Mukai T, Ishikawa K, Higashi K. High-strain-rate superplasticity in an AZ91 magnesium alloy processed by ingot metallurgy route. *Materials Transactions*. 2002. 43, 78-80.

Weerasooriya T. The MTL torsional split-Hopkinson bar. 1990. MTL-TR-90-27, U.S. Army.

Wei Q, Cheng S, Ramesh KT, Ma E. Effect of nanocrystalline and ultrafine grain sizes on the strain rate sensitivity and activation volume: fcc versus bcc metals. *Materials Science and Engineering A*. 2004. 381, 71-79.

Witkin D, Lee Z, Rodriguez R, Nutt S, Lavernia E. Al-Mg alloy with bimodal grain size for high strength and increased ductility. *Scripta Materialia*. 2003. 49, 297-302.

Yamashita A, Horita Z, Langdon TG. Improving the mechanical properties of magnesium and a magnesium alloy through severe plastic deformation. *Materials Science and Engineering*. 2001. 300, 142-147.

Yang Y, Wang F, Tan C, Wu Y, Cai H. Plastic deformation mechanisms of AZ31 magnesium alloy under high strain rate compression. *Transactions of Nonferrous Metals Society of China*. 2008. 18, 1043-1046.

Yoo MH, Morris JR, Ho KM, Agnew SR. Nonbasal Deformation Modes of HCP Metals and Alloys: Role of Dislocation Source and Mobility. *Metallurgical and Materials Transactions A*. 2002. 33A, 813-822.

Zhang Y, Topping TD, Lavernia EJ, Nutt SR. Dynamic micro-strain analysis of ultrafine-grained aluminum magnesium alloy using digital image correlation. *Metallurgical and Materials Transactions A*. 2014. 45, 47-54.

Zhao Z, Ramesh M, Raabe D, Cuitino AM, Radovitzky R. Investigation of three-dimensional aspects of grain-scale plastic surface deformation of an aluminum oligocrystal. *Int. J. Plast.* 2008. 24, 2278-2279.

Zhou W, Shen T, Aung N. Effect of heat treatment on corrosion behavior of magnesium alloy AZ91D in simulated body fluid. *Corrosion Science*. 2010. 52, 1035-1041.